TKK Dissertations 254
Espoo 2010

CRITICAL PHENOMENA IN CREEP AND DAMAGE

Doctoral Dissertation

Jari Rosti

Aalto University
School of Science and Technology
Faculty of Information and Natural Sciences
Department of Applied Physics

TKK Dissertations 254
Espoo 2010

CRITICAL PHENOMENA IN CREEP AND DAMAGE

Doctoral Dissertation

Jari Rosti

Doctoral dissertation for the degree of Doctor of Science in Technology to be presented with due permission of the Faculty of Information and Natural Sciences for public examination and debate in Auditorium K215 at the Aalto University School of Science and Technology (Espoo, Finland) on the 27th of November 2010 at 12 noon.

Aalto University
School of Science and Technology
Faculty of Information and Natural Sciences
Department of Applied Physics

Aalto-yliopisto
Teknillinen korkeakoulu
Informaatio- ja luonnontieteiden tiedekunta
Teknillisen fysiikan laitos

Distribution:
Aalto University
School of Science and Technology
Faculty of Information and Natural Sciences
Department of Applied Physics
P.O. Box 11100 (Otakaari 1 M)
FI - 00076 Aalto
FINLAND
URL: http://tfy.tkk.fi/
Tel. +358-9-47001
Fax +358-9-470 23116
E-mail: jari.rosti@tkk.fi

ISBN 978-952-60-3458-4
ISBN 978-952-60-3459-1 (PDF)
ISSN 1795-2239
ISSN 1795-4584 (PDF)
URL: http://lib.tkk.fi/Diss/2010/isbn9789526034591/

TKK-DISS-2840

Picaset Oy
Helsinki 2010

Aalto University

ABSTRACT OF DOCTORAL DISSERTATION	AALTO UNIVERSITY SCHOOL OF SCIENCE AND TECHNOLOGY P.O. BOX 11000, FI-00076 AALTO http://www.aalto.fi

Author Jari Rosti

Name of the dissertation

Critical Phenomena In Creep and Damage

Manuscript submitted 26.8.2010	Manuscript revised 26.10.2010

Date of the defence 27.11.2010

☐ Monograph ☒ Article dissertation (summary + original articles)

Faculty	Information and Natural Sciences
Department	Department of Physics
Field of research	statistical physics, disordered systems, materials science
Opponent(s)	Prof. Hans J. Herrmann
Supervisor	Prof. Mikko J. Alava
Instructor	Prof. Mikko J. Alava

Abstract

The deformation and the damage evolution are studied in creep and fracture experiments using paper samples. Experimental methods utilized are the digital image correlation and the acoustic emission. Statistical models of the deformation and fracture are tested.

In the tensile geometry, the Andrade creep phase characterized by a power law decay of the strain rate, and the increase of the relative strength of strain rate fluctuations. The integrated deformation follows a data collapse appropriate for an absorbing state phase transition. The fluctuation scaling is confirmed to exist in the logarithmic primary creep regime, but not in the creep recovery.

In the peel-in-nip geometry, under a constant force, advancing front exhibits creep-depinning phase transition. Numerical models suggest that it corresponds the motion of an elastic line with a long-range elastic interaction.

The probability distributions of the event energies, waiting times between events and the correlated dynamics of the intermittent crackling noise are studied in the fracture phenomena, in various different loading modes and loading geometries. Analogies to the tectonic seismicity is discussed.

The concept of criticality is studied in the tensile experiment and a strain imposed loading. The idea of criticality implies the presence of a divergences in the acoustic emission time series. The event rate is found to diverge, when a sample-dependent "critical time" of the maximum event rate is approached. This takes place after the maximum stress is reached. The results are compared with statistical fracture models of heterogenous materials.

Keywords plasticity, viscoelasticity, creep, disordered solids

ISBN (printed) 978-952-60-3458-4	ISSN (printed) 1795-2239
ISBN (pdf) 978-952-60-3459-1	ISSN (pdf) 1795-4584
Language English	Number of pages 151

Publisher Aalto University School of Science and Technology, Department of Applied Physics

Print distribution Aalto University School of Science and Technology, Department of Applied Physics

☒ The dissertation can be read at http://lib.tkk.fi/Diss/2010/isbn9789526034591/

Aalto-yliopisto

VÄITÖSKIRJAN TIIVISTELMÄ	AALTO-YLIOPISTO TEKNILLINEN KORKEAKOULU PL 11000, 00076 AALTO http://www.aalto.fi

Tekijä Jari Rosti

Väitöskirjan nimi

Kriittiset ilmiöt virumisessa ja vaurioitumisessa

Käsikirjoituksen päivämäärä 26.8.2010	Korjatun käsikirjoituksen päivämäärä 26.10.2010
Väitöstilaisuuden ajankohta 27.11.2010	
☐ Monografia	☒ Yhdistelmäväitöskirja (yhteenveto + erillisartikkelit)

Tiedekunta	Aalto-yliopiston teknillinen korkeakoulu
Laitos	Fysiikan laitos
Tutkimusala	tilastollinen fysiikka, epäjärjestyneet systeemit, materiaalitieteet
Vastaväittäjä(t)	Professori Hans J. Herrmann
Työn valvoja	Professori Mikko J. Alava
Työn ohjaaja	Professori Mikko J. Alava

Tiivistelmä

Paperin muodonmuutosta ja vaurion kehittymistä tutkitaan virumisessa sekä murtokokeissa. Työssä sovelletaan kokeellisina menetelminä kuvakorrelaatiota ja akustista emissiota. Kokeellisia tuloksia verrataan tilastollisiin malleihin.

Tasogeometriassa tehdyssä virumiskokeessa, jossa havaitaan Andraden virumislaki, virumisnopeuden paikalliset vaihtelut kasvavat. Andraden virumisessa venymä kasvaa verrannollisesti ajan kuutiojuureen, kun taas vaihtelut kasvavat verrantona ajan neliöjuureen. Integroidun muodonmuutoksen venymäjakaumafunktiot noudattavat skaalausta, jonka mukaan Andraden viruminen voidaan tulkita absorboivan tilan faasimuunnoksena. Virumisnopeuden paikallisten vaihteluiden voimistuminen havaitamaan myös logaritmisessa primäärisessä virumisessa, mutta ei virumisen palautumisessa.

Halkaisugeometriassa vakiovoimalla etenevä murtorintama noudattaa virumis-jumiutumis faasimuutoksen tilayhtälöä. Numeeristen mallien avulla voidaan päätellä, että murtorintaman elastisuus voi olla luonteeltaan pitkän kantaman vuorovaikutus.

Purskeisen murtomelun energian ja odotusaikoijen todennäköisyysjakaumia, sekä sen korreloitunutta dynamiikkaa tutkitaan käyttäen erilaisia murto- ja kuormitusgeometrioita. Paperin murtumisen yhdenmukaisuutta seismisyyteen vertaillaan.

Ilmiön kriittisyyttä tutkitaan laajoin kokein tasogeometriassa vakiovetonopeudella. Purskeisuuden - "järistyksien lukumäärän" - havaitaan hajaantuvan, kun näytekohtainen kriittinen piste saavutetaan. Kriittisen pisteen havaitaan sijaitsevan eri paikassa, kuin voima-venymä-käyrän maksimijännitys. Tuloksia vertaillaan epäjärjestyneen aineen murtomalleihin.

Asiasanat plastisuus, viskoelastisuus, viruminen, viskoelastiset materiaalit

ISBN (painettu) 978-952-60-3458-4	ISSN (painettu) 1795-2239
ISBN (pdf) 978-952-60-3459-1	ISSN (pdf) 1795-4584
Kieli englanti	Sivumäärä 151

Julkaisija Aalto-yliopiston teknillinen korkeakoulu, teknillisen fysiikan laitos

Painetun väitöskirjan jakelu Aalto-yliopiston teknillinen korkeakoulu, teknillisen fysiikan laitos

☒ Luettavissa verkossa osoitteessa http://lib.tkk.fi/Diss/2010/isbn9789526034591/

Preface

I acknowledge the financial support of the COMP, Academy of Finland, Väisälä Foundation and the European Commission NEST Pathfinder programme TRIGS under contract NEST-2005-PATH-COM-043386.

I wish to express my gratitude to my instructor Prof. Mikko Alava for the guidance and support. I am also very grateful to him for getting this intriguing topic, which was linked to the topical research, but at the same time it was connected to the open problems that had fascinated physicists for centuries.

I am grateful to my coauthors for the collaboration, especially Lauri Salminen, Juha Koivisto and Lasse Laurson. All the colleagues and students at the CSM group from past to present are thanked for creating the inspiring atmosphere. I thank my colleagues in the COMP and persons who created its facilities supporting the research. It is a pleasant work environment.

I sincerely thank the pre-examiners Dr. Juha Merikoski and Prof. Michael Zaiser for careful checking of the manuscript as well as constructive feedback. I thank FM Elina Anttila for proofreading the thesis.

Otaniemi, 3.11.2010

Jari Rosti

Contents

List of Publications

This thesis consists of an overview and of the following publications which are referred to in the text by their Roman numerals.

I Jari Rosti, Juha Koivisto, Lasse Laurson and Mikko J. Alava, *Fluctuations and scaling in creep deformation*, Phys. Rev. Lett. **105**, (2007) 100601.

II Mika Mustalahti, Jari Rosti, Juha Koivisto and Mikko J. Alava, *Relaxation of creep strain in paper*, J. Stat. Mech. **P07019**, (2010) 1-19.

III Jari Rosti, Juha Koivisto and Mikko J. Alava, *Statistics of acoustic emission in paper fracture: precursors and criticality*, J. Stat. Mech. **P02016**, (2010) 1-18.

IV Lauri I. Salminen, Joonas M. Pulakka, Jari Rosti, Mikko J. Alava and Kaarlo J. Niskanen, *Crackling noise in paper peeling*, Europhys. Lett. **73**, (2006) 55-61.

V Juha Koivisto, Jari Rosti and Mikko J. Alava, *Creep of a fracture line in paper peeling*, Phys. Rev. Lett. **99**, (2007) 145504.

VI Jari Rosti, Juha Koivisto, Paola Traversa, Xavier Illa, Jean-Robert Grasso and Mikko J. Alava, *Line creep in paper peeling*, Int. J. Fract. **151**, (2008) 281-297.

Author's contribution

The Author has had an active role in designing and developing the measurement environment and designing the experiments in publications I-IV and VI.

In Publication I, the Author adapted the DIC method for analyzing the experiments and performed most of the experimental analysis work. The Author contributed in writing the experimental parts of the article.

In Publication II, the Author contributed to the design of the experimental work, performed the spatiotemporal strain field analysis, and wrote the corresponding parts of the manuscript. The Author contributed by performing part of the analysis for the landscape model presented in the manuscript, and had an active role in writing the manuscript.

In Publication III, the Author performed the experiments, did the experimental analysis work, implemented the numerical model and analyzed the numerical experiments. The Author was responsible for writing the manuscript.

In Publication IV, the Author performed the correlation analysis presented in the manuscript.

In Publication V, the Author supervised the experimental work and contributed to the design of the experiment.

In Publication VI, the Author performed the correlation analysis and was responsible of writing the corresponding part in the manuscript. The Author contributed to developing joint analysis methods for seismicity and paper peeling experiments.

1 Introduction

When a material is subjected to a long-term exposure of stress below the yield strength it deforms. The deformation is called creep. It is related to the structure of a material, its temperature and, specifically for paper as a material, environmental conditions such as humidity. The creep can lead to the catastrophic failure of a material and it is a source of concern to engineers designing structures operating under considerable stresses and high temperatures.

The science of the creep in engineering is based on empirical laws of creep deformation [1, 2, 3, 4, 5, 6]. How phenomenological laws emerge from a collective behaviour of constitutive elements, is a question that is in the domain of statistical physics. A system driven by stress is not in equilibrium. In statistical physics, tools for non-equilibrium systems evolved from phase transitions of equilibrium systems, and there are two fundamental concepts: scaling and critical fluctuations [7, 8, 9]. The scaling means that under a transformation essential properties of statistical distributions describing the system remain unchanged. Critical fluctuations are a consequence of a lack of a length scale other than the system size and the atomic scale. Fluctuations emerge as scalefree features of the probability distributions describing the system.

Statistical physics approach has been used in various ways in order to understand the phenomenology of material failure under stress, for example, fractal scaling of fracture surfaces [10, 11, 12, 13, 14] and critical fluctuations in tectonic seismicity leading to Gutenberg-Richter and Omori's laws [15, 16]. The essential ingredient in understanding the material failure is the role of flaws and the disorder present in the structure. This was first highlighted by Leonardo Da Vinci when he studied the strength of metal wires [17, 18]: which led to a concept that one must describe the structural flaws instead of the ideal structure in order to understand the size effect of the material strength [19, 20].

In this thesis we use paper as a test material, a quasi two-dimensional system with intrinsic structural disorder [21, 22, 23]. We use statistical physics tools to develop the understanding - how phenomenological laws emerge - for creep phenomena and catastrophic failure of material. Creep, creep recovery and damage evolution are studied in this thesis by performing experiments on ordinary paper sheets.

The study of creep, creep recovery and damage, presented in this thesis, is an approach to understand this non-equilibrium phenomena of the deformation. As an example, Andrade's phenomenological creep law states that the deformation rate decays in time as a power law originates from 1910 and its theoretical roots are under a debate [24, 25]. Creep is classically considered as a viscous flow of a material. The picture of a smooth plastic flow process has changed through studies of crystalline materials, based on experimental and theoretical advancements [26, 27, 28, 29].

The creep and recovery experiment is performed by using the Digital Image Correlation (DIC) method, from which we obtain a spatio-temporal evolution of the strain. The damage evolution under stress is studied by using acoustic emission, the crackling noise, in conjunction with the strain. Acoustic emission (AE) is an intermittent noise generated by sudden release of the stress [30, 31] and the intermittent nature of AE is understood via many statistical models of fracture [32, 33]. In this work, general statistical properties of AE are studied in detail by using experimental setups with different loading modes and loading geometries and experiments are compared with numerical experiments on different models.

The main contribution of the thesis is that the Andrade's creep on paper related to a jamming or absorbing state phase transition. The strain evolution is studied in the framework of elastic interface depinning. The analysis is based on a method of analyzing spatiotemporal strain fields during the creep experiment, using the digital image correlation method. Moreover, it is shown that the creep recovery, although it has functional form analogous to that in Andrade's creep, does not fit the same

interfacial picture. This result is verified by studying the fluctuation scaling law of spatial strains. However, the origin of the fluctuation scaling remains unexplained.

We contribute to the understanding of the catastrophic failure of material. There are discrepancies in the literature concerning the nature of the damage accumulation [34] and this issue is studied by using numerical and experimental methods. Specifically, we concentrate on the differences between the event and the energy rates during the damage accumulation. Moreover, non-stationary aspects of damage accumulation during paper fracture are compared with results of stationary experiments. Analogies to seismicity are discussed. The results are contrasted to numerical experiments.

The outline of this thesis is as follows. In Chapters 3, 4 and 5 we present background information and a qualitative description of the phenomena under study. In Chapter 5 we present the experimental methods. In Chapter 6 we discuss the main observations and their implications. In Chapter 7 we present our conclusions.

2 Creep deformation

Fundamental work on creep has been done by E. Andrade 1910 [24], where he observed that after some time, an extension of a lead or metal wire becomes proportional to the time, and viscous in character. Andrade studied how the rate of the viscous flow varies with the load. The measurement setup is shown in Fig. 2.1. He found the empirical relation

$$l = l_0(1 + \beta t^{\frac{1}{3}})e^{kt}, \tag{2.1}$$

where l is the length of the wire. The parameter l_0 characterizes the instantaneous elongation of the sample. The phenomenological creep law was divided to the β-flow, characterized by a parameter β, and the viscous flow due to an exponential term e^{kt}. The β-flow is more commonly observed in the "high temperature" case [24]. This established the phenomenological division of creep deformation under a *constant stress* where, the β-flow, or the initial power law decrease of strain rate, is called primary creep. This is followed by a quasistationary regime, secondary creep, where the change in the creep deformation rate is approximately constant, and transitions eventually to a tertiary, final creep which leads to catastrophic failure of the material. The β-flow, the power-law primary creep, was later to be known by its inventor: Andrade's law, which is in terms of the creep deformation

$$\epsilon(t) = \epsilon_0 + \beta t^p, \tag{2.2}$$

where $\epsilon = l/L$ is the strain, ϵ_0 is initial strain, β is the free parameter and p is an exponent and its particular value 1/3 is coined as Andrade's creep.

Andrade's law has been found for various materials, from metals with a crystalline structure to polymeric materials [4], from composites [35] to rocks [36], polycrystalline ice [37] and ordinary paper sheets [38]. The most extensive study was done by Crussard on various crystalline materials with different metallurgical treatments

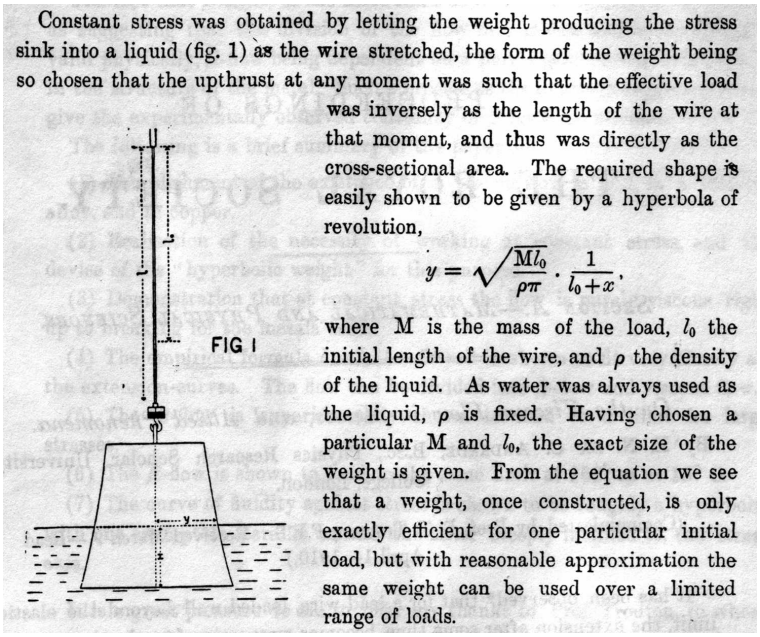

Constant stress was obtained by letting the weight producing the stress sink into a liquid (fig. 1) as the wire stretched, the form of the weight being so chosen that the upthrust at any moment was such that the effective load was inversely as the length of the wire at that moment, and thus was directly as the cross-sectional area. The required shape is easily shown to be given by a hyperbola of revolution,

$$y = \sqrt{\frac{Ml_0}{\rho\pi}} \cdot \frac{1}{l_0+x},$$

FIG 1

where M is the mass of the load, l_0 the initial length of the wire, and ρ the density of the liquid. As water was always used as the liquid, ρ is fixed. Having chosen a particular M and l_0, the exact size of the weight is given. From the equation we see that a weight, once constructed, is only exactly efficient for one particular initial load, but with reasonable approximation the same weight can be used over a limited range of loads.

Figure 2.1: The measurement setup by Andrade for measuring the creep of lead and metal wires. A hyperbolic weight in a liquid is used to vary either constant stress or constant load applied to the sample. Removing liquid slowly in the beginning of the experiment also guaranteed smooth and steady application of the load during the initial stages of the experiment and allowed to use a large stress, which is necessary for Andrade's creep. By permission of the Royal Society, from Ref. [24], p. 2, Fig 1.

[39]. Experiments show that the transient creep regime shows a power law dependence according to Eq. (2.2), but the exponent p is not universal, ranging from 0, corresponding a logarithmic creep, up to values close to 1 [25]. A historical viewpoint is presented by Crussard in Ref. [40] and Fig. 2.2 shows experimental data by Cottrell [41]. An open question is, whether the variations in the exponent are due to physical reasons or experimental uncertainties, and a review of the current state of matters is presented in Ref. [25].

For metals, theoretical approaches are proposed which explain Andrade's exponent 1/3 via interacting dislocations. Mott's statistical theory relies on assumptions based on collective dislocation activity, which leads to description for the work hardening

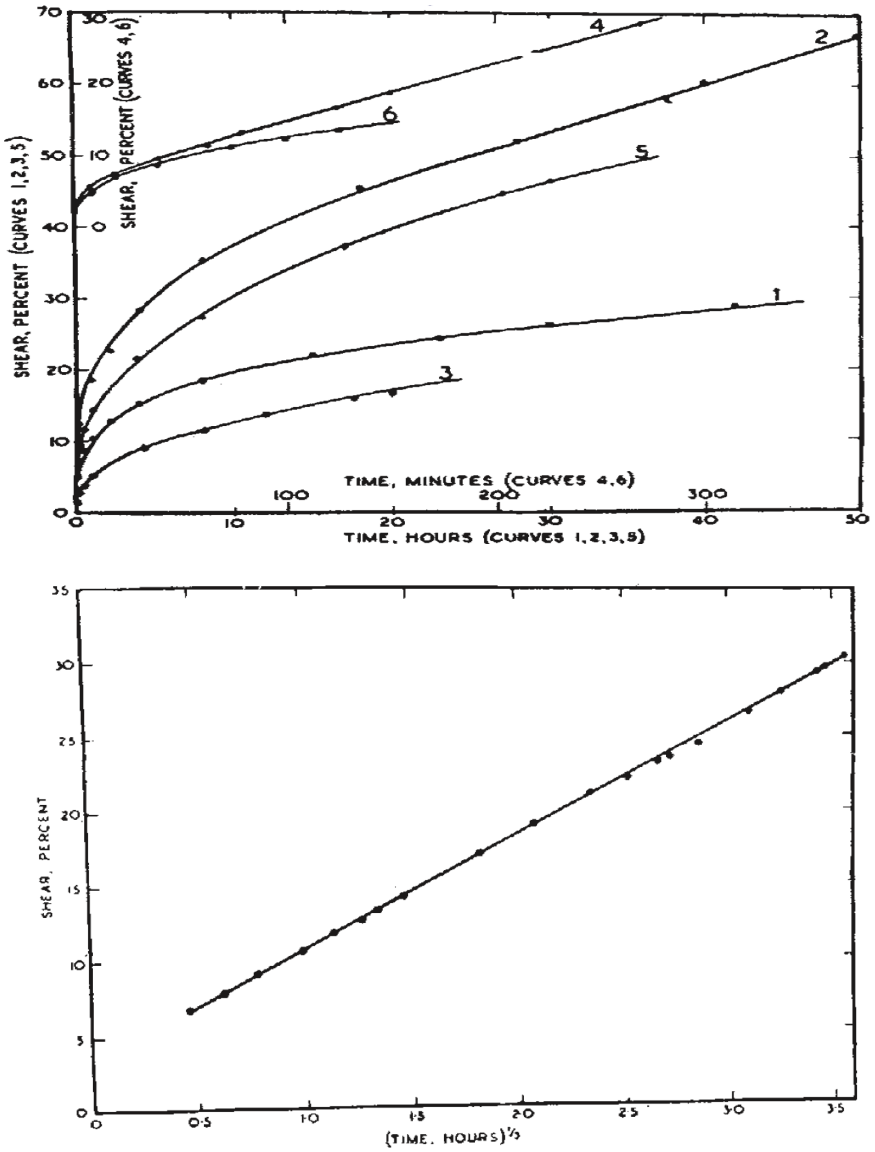

Figure 2.2: Upper panel: creep of zinc crystals under constant shear stress. Solid lines are from a fit $\gamma = \gamma_0 + \beta t^{1/3} + \chi t$, where γ is the shear at time t and γ_0, χ and β are free parameters. Lower panel: Test of the β-flow on specimen 1, where χ was found to be zero. By Permission of the Nature Publishing Group, From Ref. [41].

and the recovery. The strain of the system is proportional to the dislocation movement. It assumes that the activation energy U_β of the Andrade creep phase is 1/3 of the activation energy in the linear creep regime. Cottrell's microscopic model assumes that dislocations can overcome obstacles and move, due to a load shedding or a thermal activation. A time scale associated with movement due to load shedding is shorter than a time scale induced by thermal activation. This creates collective dislocation movements, where strain bursts are created due to the mechanical load shedding. Avalanches are initiated by a thermal activation event. A common aspect to both models is linear hardening, that is on a point of a stress-strain curve of a material, where the creep strain is ϵ, the hardening $\Delta\sigma$ due to the strain is linearly proportional to the strain,

$$\Delta\sigma \sim \epsilon.$$

It is argued that Andrade's particular value of the exponent, 1/3, is attributed to the cases where the linear work hardening assumption is valid. [42, 43, 25]

Cottrell computed the total number of mechanical triggerings of dislocation cascades N_m. He divided the system to "cages" and defined a "reproductive factor k" , i.e. the average number of "obstacles" in a cage that are mechanically triggerable by a load sched. The average number of mechanically triggerable events due to a thermally activated event is a sum

$$N_m = \sum_{i=0}^{\infty} k^i - 1 = \frac{k}{1-k},$$

where i indicates a generation of the cascade. When $k = 1$ the expression is divergent, that is a single thermally activated event is able to trigger an infinite number of dislocation movements. At point $k = 0$ all activity is thermally activated, and the system is in the linear creep regime. This divergence is reminiscent of critical phenomena, where Andrade's creep is the transient when systems moves away continuously from the critical state towards the linear creep regime. Related to the arguments by Cottrell and Mott, the evidence of the intermittent nature of the creep strain has emerged, and collective phenomena of dislocations have recently caught the attention in the statistical physics community [44, 27, 29, 45, 46].

Andrade's transient is observed in 2D discrete dislocation dynamics models (DDD) [44]. The DDD model is a cross section of a single crystal with straight parallel edge dislocations gliding along a single slip direction parallel to their Burgers vectors $\vec{b} = \pm b\vec{u}_x$. Point-like edge dislocations move under the influence of an external stress σ, and interact via a long-range anisotropic interaction

$$\sigma_s(\mathbf{r}) = Dbx\frac{x^2 - y^2}{(x^2 + y^2)^2}, \tag{2.3}$$

where $D = \mu/2\pi(1 - \nu)$, with μ the shear modulus and ν the Poisson ratio of the material. Coordinates (x, y) refer to a plane, which is perpendicular to a dislocation line. A critical value σ_c of the shear stress means that the average dislocation velocity $\langle v\rangle$ decreases as a power law, as a function of time

$$\langle v\rangle(t) \sim \langle \epsilon_t\rangle(t) \sim t^{-\theta}, \tag{2.4}$$

which is the time-derivative ($\frac{d\epsilon(t)}{dt} \equiv \epsilon_t$) of Eq. (2.2). The exponent $\theta = 1 - p = 2/3$ is found from the DDD model. The features of the phase transition in the DDD model are similar to the jamming phase transition seen in granular media and glasses [47, 48, 49]. That is, in the DDD model transition to the linear creep is controlled by jamming: dislocations form metastable configurations, and the dynamics advances through absorbing states. Contrary to Cotrell's microscopical model, in DDD a thermal activation has no role in the Andrade's creep behaviour. An important ingredient in the model, not present in the analytical arguments by Mott and Cotrell, is the explicit long-range and anisotropic nature of the interactions. [50, 51, 52]

A study by Daehn uses cellular automata on a 2-dimensional lattice [53]. In the model "plastic slips" are accumulated in each site, which are thermally driven events based on an expression for the activation energy. The stress relaxation is introduced by balancing it to with nearest neighbours. The stress redistribution rule creates cascading strain avalanches, in similar vein as sandpile models show an intermittent activity [54]. The model has a strain versus time transient between two steady state (linear creep) regimes, and the transient may be described by Eq. (2.2). The CA

does not rely on a concept of a dislocation, and thus the approach may be applicable to describing creep of non-crystalline materials.

The arguments based on thermal activation, Cotrell's microscopic theory, Daehn's cellular automata and numerical experiments on DDD are all able to produce Andrade's creep. The latter three are based on microscopical arguments, with different physical assumptions on the origins of creep. In Daehn's cellular automata and in Cottrell's theory, strain bursts are due to the design of the model: the cascades emerge from driving the system by a thermal activation. The interactions between dislocations are short-ranged, or at least the models do not imply a long-range interaction. In DDD simulations avalanches are directly due to the collective dislocation activity. Jammed states emerge due to slip plane geometry restrictions, and an anisotropic and long-range interaction. Strain bursts occur, when the system enters from the metastable state to another.

The surface profiles of plastically deformed crystals have been observed to develop self-affine roughness with non-trivial roughness exponent $H = 0.8$, suggesting fluctuations in the deformation [55]. A continuum model has been proposed by Zaiser and Moretti, and for parallel edge dislocations an expression is derived, which describes the motion of an elastic manifold through a disordered medium inducing a fluctuating pinning force to the manifold according to an equation

$$\sigma_{ext} + \sigma_{int}(\vec{r}) + \frac{DG}{\rho}[\gamma_{xx} + \gamma_{yy}] + \delta\tau(\vec{r}, \sigma) = 0, \tag{2.5}$$

where D is a constant near unity, G is the shear modulus, γ is the shear strain, $\delta\tau$ is a quasi-static random pinning field and σ_{ext} and σ_{int} are an external and an internal stress respectively. Zaiser and Moretti show that, despite the differences from conventional models of elastic manifolds, the model shows depinning-like behaviour. [26]

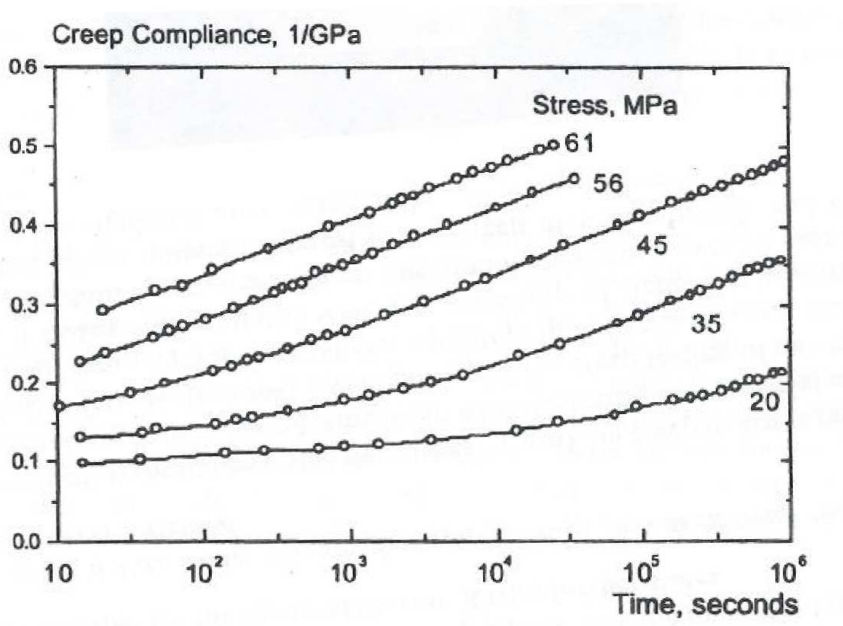

Figure 2.3: Creep compliances $\epsilon(t)/\sigma$ of paper. Experiments show the logarithmic creep spanning several decades in time on the primary creep region. By permission of TAPPI, from Ref. [38].

The logarithmic creep deformation

$$\epsilon(t) = K \log(t) + D \tag{2.6}$$

has been found to be valid for the primary creep [37, 39, 38]. Logarithmic creep can be explained by the exhaustion theory in which regions with low activation energies yield, leaving the regions of higher energy to activate later. However, thermal activation arguments are also extended to comply with a power law primary creep according to Eq. (2.2), or with an indistinguishable exponent [56, 57, 58, 36]. In Fig. 2.3 a creep compliance from paper samples is shown, where a logarithmic creep region over several decades is seen [38].

In paper, experiments reveal all phenomenological phases of creep [2, 59]. The secondary creep stage in polymers and paper does not show a constant creep rate regime, but rather the creep rate decreases until the tertiary regime. According to

the usual definition, the secondary creep is not attributed to the constant strain rate, but it is commonly defined that the primary creep is recoverable, while the secondary one is not [2, 38]. A creep curve is shown in the Fig. 2.4, which shows typical creep behaviour of paper. Early guesses about the mechanism of creep made by Brezinski [38] and Van den Akker [60] suggested that the events inside the fibre would be mainly responsible for the creep phenomenon. This idea was contradicted later, and it is believed that interfibre events are the driving force in the creep phenomenon [61]. The engineering literature on paper does not suggest an intermittent strain evolution, nor "collectivity" in the physical description of creep, as it is for crystalline materials via the dislocation picture. Phenomenological laws on creep in paper are established, but a quantitative connection between microscopic origins and phenomenology is lacking.

A typical experimental setup of a creep study, e.g. by Andrade, measures the global strain of the sample as a function of time. In this thesis, we take an alternative approach to looking at the problem: the spatial structure of strain during the creep. Schematically our experimental approach is shown in Fig. 2.5.

The main motivation of the experimental approach in this work is to develop accurate measurement of the spatiatemporal strain field during creep experiment and study its implications on creep, and the models described. The strain field is illustrated schematically in Fig. 2.5, and the computation of the strain from the displacements is shown in the Chapter 6. Spatial strain rates are observable in the DDD model, and we achieve further understanding about the idea of jamming transition applied to non-crystalline materials. The spatiotemporal evolution of the strain during primary creep and its implications is studied in Publication I.

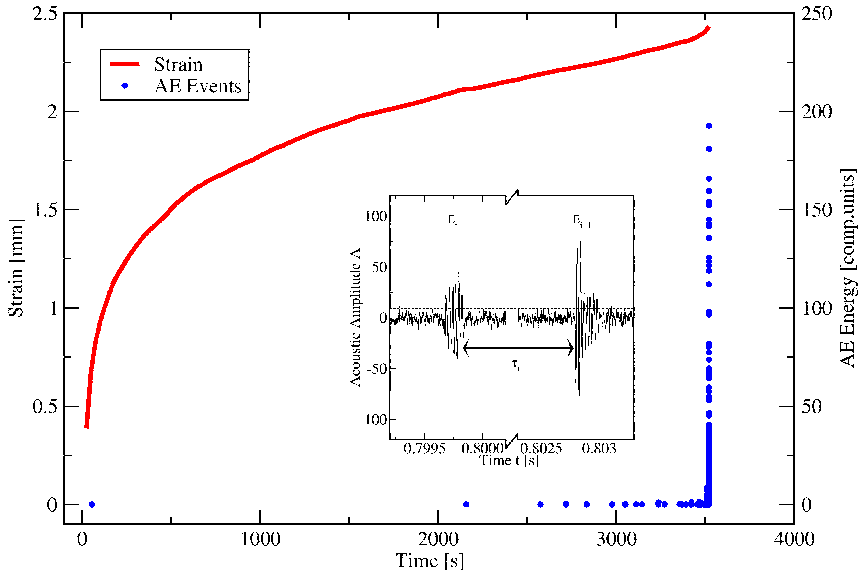

Figure 2.4: Typical time vs. strain curve from tensile creep experiment. The curve shows the total strain of the sample, and the dots indicate acoustic emission events during the experiment, with the energy scale indicated on the right. Inset: zoom to the acoustic emission signal, where we observe two consecutive events with energies E_i and E_{i+1} and a waiting time τ_i. This figure shows a typical creep behaviour of paper, with the three phases (primary, secondary, tertiary). It also indicates the relative absence of the crackling noise, that is the small number of acoustic emission events (AE) during the primary (no events) and secondary creep of the sample.

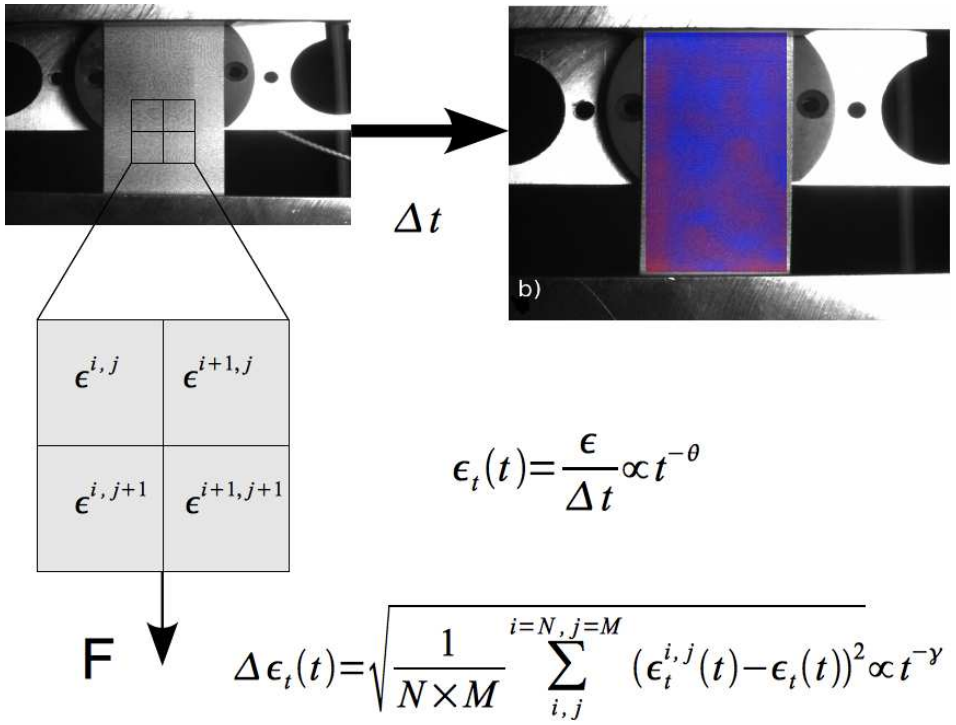

Figure 2.5: A time-series of displacement fields is derived from consecutive images taken from a sample under stress at time interval Δt. From the displacement fields one can measure spatial strains $\epsilon^{i,j}$ and spatial strain rates $\epsilon_t^{i,j}$. The equation for the standard deviation $\Delta\epsilon^{i,j}$ is shown. Superposed on the upper right image is a typical deformation grid for a time difference Δt of 10 seconds. The color scale indicates the degree of local creep deformation (blue: small, red: large). In the background: the experimental setup. The visible speckle pattern is printed and designed to have a structure and contrast appropriate for the DIC method. (Publication I)

3 Creep recovery

The creep response exhibits a recovery phenomenon after the removal of a stress. Despite the fact that a simple power law form for the recovered strain rate has been found for polymers in extremely long term creep-recovery studies [62] and for the polycrystalline ice [37] amongst others, the recoverability of the materials is not properly described by any microscopic model. For example, models for crystal plasticity applicable to the primary creep have difficulties in describing the recovery phenomena [26].

Semi-empirical viscoelastic models treat creep and creep recovery via constitutive elements. The most simple models describing viscoelastic materials are the Maxwell model and the Kelvin model. The Maxwell model consist of a spring and a dashpot connected in series. The spring describes an ideal elastic material while the dashpot describes an ideal viscous material [3].

The method for measuring spatial strains during creep is extended to accurate study of the recovery of the paper sample. The method allows us to put typical viscoelasticity models under a test (on paper). Fig. 3.1 shows a creep-recovery curve from experiments. The recovery can be divided in the initial recovery and the delayed recovery. The former occurs immediately after removing the load, while the latter is characterized by an extremely slow response.

Via an empirical energy landscape fitting model, we can estimate the form of the activation energy expression during the recovery. If we write the recovered strain rate equal to the strain times by a typical relaxation rate

$$\partial_t \epsilon = -E\epsilon/\tau,$$

where E is the elastic modulus and τ is the relaxation time, it would imply an exponential decay. To capture the extremely slow response, we can study the expression

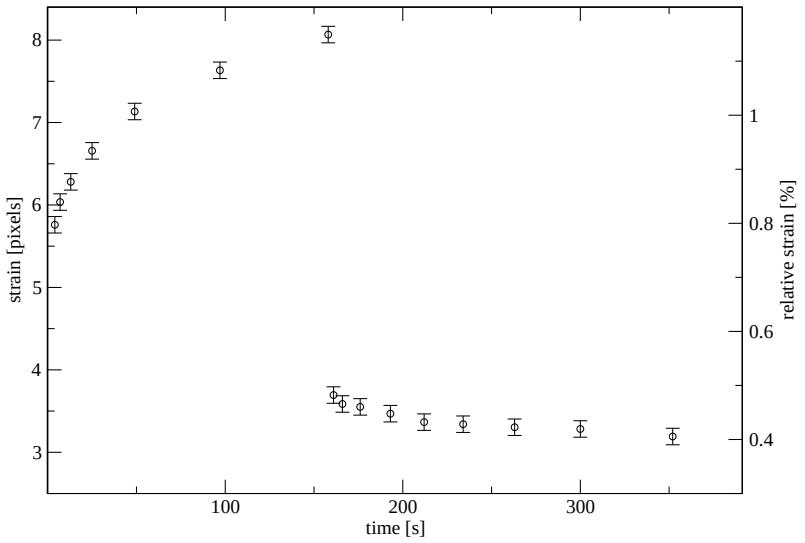

Figure 3.1: A typical example of the deformation curve in a creep-recovery experiment. The total strain is computed as the total displacement of the image area to the strain direction using a displacement field obtained from DIC. Error bars indicate a 0.1 subpixel limit. Pixel size is 4 μm. In the creep regime the sample deforms according to Andrade's law with an exponent $\epsilon(t) \sim t^{0.1}$. (Publication II)

of a typical barrier $U(\epsilon)$, which governs the relaxation at a given time.

Finally, the spatial recovery behaviour can be compared to the spatial strain fields obtained from the primary creep, and we get the behaviour of the spatiotemporal strain evolution in two fundamentally different experimental scenarios: if one considers the creep strain evolution as a jamming transition, one must assume that the stress is near the critical value.

The results of the creep recovery study are reported in Publication II.

4 Damage evolution and acoustic emission

Acoustic emission (AE) is an experimental method of studying the damage evolution. AE is caused by the sudden release of elastic energy due to microcracking on various scales and it is an evidence of the intermittency during the deformation of the material. In this chapter, we extend our discussion from creep deformation, and discuss general properties of AE during fracture of materials.

AE studies have been done on a wide variety of materials in science and in engineering [63]. In engineering AE is applied as a non-destructive testing method in addition to characterizing failure from various materials [64, 65, 66].

In the paper research acoustic emission was initially studied by Corte and Kallmess [67] in the audible frequency domain, and later more extensively by Yamauchi et al. [68, 69, 70] with a succesful source localization, Gradin et al. for characterizing material properties, e.g. fracture toughness [71]. Rosti et al. and Salminen et al. studied the scale-free statistics of AE [72, 73]. The observations on paper were not novel in materials research in general: the first observation of the scale-free statistics of AE originates from 1962 by Mogi [74] (see Fig. 4.1), and the critical dynamics in fracture was first suggested by Petri et al. [75].

The acoustic emission data consist of a set of events. An example of an acoustic emission event is shown in the inset of Fig. 2.4. The event is characterized by its energy E_i and arrival time t_i. The probability distribution function of the event energies and the silent time $\tau_i = t_{i+1} - t_i$ integrated over a fracture experiment exhibit almost without exception power-law statistics which are characterized by power-law exponents α and β [75, 30, 76, 77, 34, 78], respectively, according to equations

$$P(E) \sim E^{-\beta} \tag{4.1}$$

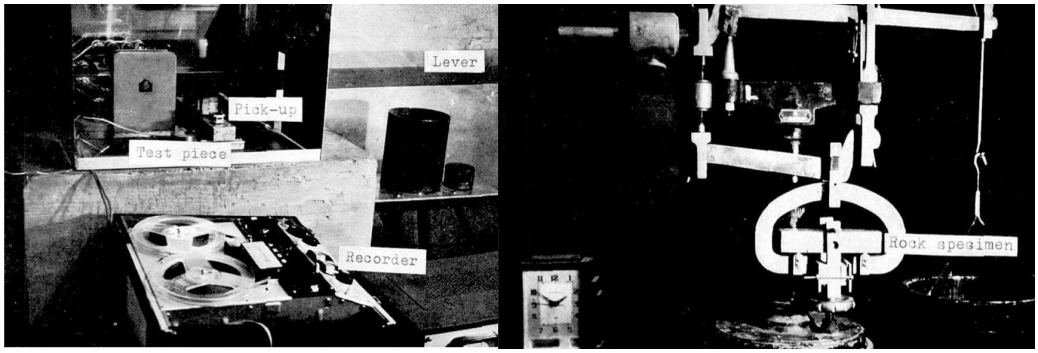

Figure 4.1: The acoustic emission measurement device by Mogi. The device was used to record the first observation of "Gutenberg-Richter" law according to Eq. (4.4) from a microcracking experiment. The "shock events" were obtained by bending rock samples. From Ref. [74].

and

$$P(\tau) \sim \tau^{-\alpha} \tag{4.2}$$

with a large scatter in exponents, $\beta = 1.2 \ldots 1.8$ and $\alpha = 1.0 \ldots 1.5$.

The density of the event energy increases when the catastrophic failure is approached. The signature of the acoustic emission is non-stationary. This time-to-failure acceleration of the energy rate has been suggested to diverge in creep test:

$$E_t(t_c - t) \sim (t_c - t)^{-\Gamma}, \tag{4.3}$$

where E_t is an energy rate respect to time, t_c is the time to failure and Γ is the exponent which characterizes the acceleration, with a value 1.3...1.5 [79, 80, 81]. In contrast to the divergence, strain-controlled experiments on paper show an exponential increase in the event energy and show no divergence in the event rate [76]. Statistical fracture models either do not indicate any (energy) divergence at all, or in the case of "democratic fibre bundles", imply a power-law with a fixed exponent and an increasing cut-off [34, 32]. A plausible question is, how exponents β and α, and the divergence signature Γ - if it exists - depend on the way how the stress is

applied [82, 83, 84, 85]. The form of the probability distribution functions may be related to the non-stationarity of the AE signal and the same applies to the time to failure acceleration. Publication III discusses the aspects of non-stationarity in acoustic emission during fracture, in particular the test for critical divergences, on the basis of a large dataset of paper fracture experiments. It contrasts the result to the numerical experiments of random fuse model with a residual conductivity, where one finds an acceleration of the event rates during a numerical experiments, but no divergence.

In contrast to non-stationarity of loading modes, in the peel-in-nip geometry (see Chapter 5, Fig. 5.2) the fracture process is stable and has a translational invariance in time [86, 87]. In this geometry the fracture front - 1D-dimensional crack propagation - is shown to propagate with intermittent jumps by a direct observation, using a high speed camera and a transparent plexiglass sample [86]. The dynamics of the fracture front may be understood via the theoretical picture of the depinning of an elastic manifold in random media [88]. Depinning has experimental realizations for example as domain walls of Ising systems and vortices in superfluids [89, 90, 91], and observations are predicted by theoretical calculations based on the functional renormalization-group approach [92, 93, 94]. The peel-in-nip is thus a useful approach to study the damage evolution by using the acoustic emission method: there are diverse experimental setups and theoretical approaches to compare with.

Publications IV and V study the peeling geometry in both the stationary strain rate and in creep mode of loading. Statistical properties of AE from peel-in-nip, in particular the correlations, are contrasted with the non-stationary data sets obtained from tensile loading geometries. The creep depinning hypothesis in 1D fracture front propagation is tested in Publication IV.

Seismicity is characterized by empirical Gutenberg-Richter law for the size distribution of earthquakes. The law states that the probability distribution for the

magnitude M is

$$P(M) \sim M^{-\beta}, \tag{4.4}$$

where $\beta \approx 1.5$. Temporal characteristics are described by Omori's law $r_t \sim (t_r - t)^{-\Pi}$, which states that the average density of earthquakes r_t increases as a power-law with an exponent Π, when we approach up to a main-shock, which occurred at a time t_r. [15, 16]

There is an analogy between empirical relations for fracture, stationary driven crack fronts and for seismicity, but the connection is not understood quantitatively nor qualitatively. Moreover, a quantitative theoretical explanation for exponents $\alpha, \beta, \Gamma, b, \Pi$ is lacking, and the statistical signatures imply complex correlations in the acoustic emission signal [84].

Publication VI discusses the analogy between seismicity and paper peeling. The methodology developed for seismicity is applied to AE from paper peeling and vice versa. Correlations in the AE from the creep in peeling are studied. The results are compared to the numerical model of the elastic interface depinning.

5 Experimental methods

In the experiments, a sheet of paper in tensile and peeling geometries was tested. Tests were made under humidity and temperature controlled conditions. Constant strain rate was applied using MTS/400M tensile testing machine for both experimental geometries. In the creep loading mode a constant load was applied on the sample.

In Publications I-III samples were tested under tensile stress using creep, creep-recovery and strain controlled modes of loading. An example of an experimental setup in tensile geometry and creep experiment is shown in the Fig. 5.1. The experimental setup for the tensile creep was constructed. It consisted of a sturdy frame, clamps, a jig to attach the sample to the clamps, and a pneumatic mechanism to apply or remove the load to the sample. A camera was attached to the frame, and a laser distance sensor followed the movement of the lower clamp. Experiments performed in publications III-VI were carried in the peel-in-the nip geometry. A paper sample under peeling is shown in the Fig. 5.2. The peel-in-nip device consisted of two rotating rolls, a wire to rotate both rolls with either a constant strain rate or a constant force. The angle of the peeling paper was followed by taking pictures during the experiment. Two acoustic emission sensors were attached to the system.

The data in the experimental setup consisted of the AE signal, the sample elongation, force and digital images. The measurement environment consisted of a standard PC hardware and networked measurement software, which coordinated the experiment and collected the data from different sources. The synchronization of different data sources was handled by using an internal counter of 1.2 MHz PCI-MIO data acquisition card that was used as a universal time for the environment. An order of 10 μs temporal accuracy between the data sources was achieved. The messaging between different parts of the measurement system were distributed us-

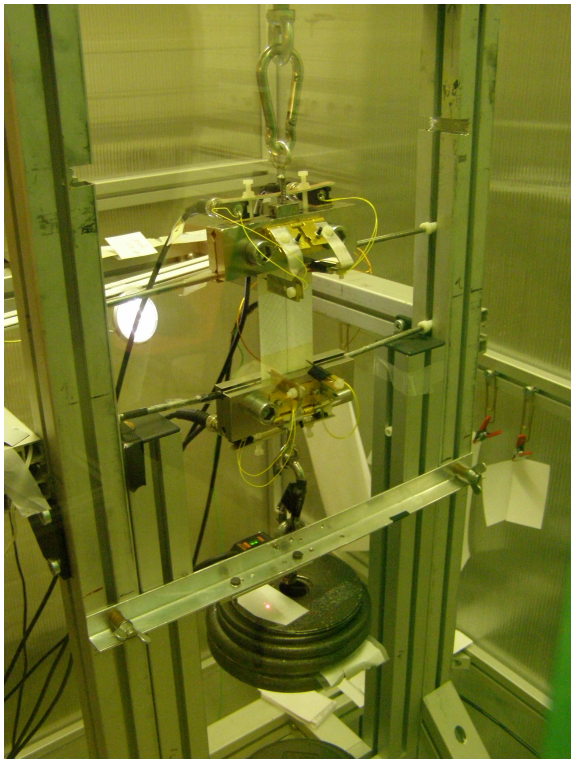

Figure 5.1: The setup for creep and creep recovery experiments. A load is attached to the lower clamp and its movement is controlled by using pneumatic cylinders. During the recovery phase the pneumatic cylinders let the sample recover freely without any load. (Publication II)

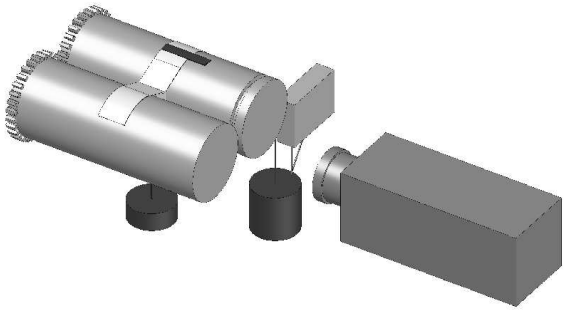

Figure 5.2: Schematic presentation of the peel-in-nip device. A paper sample is attached between two rolls. By rotating the rolls the sample peels. (Publication IV)

ing UDP/IP protocol and thus we were able to control the networked measurement hardware in a synchronous manner.

The experimental setup consisted of two special techniques, the acoustic emission analysis and the digital image correlation. The acoustic emission analysis developed by Salminen [73] was combined with the digital image correlation (DIC) measurement setup.

The images for the DIC were taken during the experiment with PCO's 1 mega pixel grayscale digital camera, SensiCam 370KL0562. The camera has a very low thermal noise ratio due to the cooled CCD and 12 bit grayscale resolution. The exposure time in most measurements was adjusted to be 200 ms, which filtered out external oscillations in lightning conditions.

Several lightning conditions and speckle patterns were tested in order to obtain the best achievable sharpness to images. Two different approaches for imaging was used: a sample scale and a fibre scale. In sample scale images, the speckle pattern shown in diagram 2.5 was used due to its sharp contrast and translational invariance. In fibre scale imaging, the natural disordered pattern of paper fibres was sufficient to create enough contrast for the DIC-method.

5.1 Digital Image Correlation

In this subchapter we discuss the digital image correlation (DIC) method and its applicability to study paper creep under deformation.

In the DIC method, the task is to find corresponding points, the deformation function, between two images. The deformation function is the mapping from a point r in the original image to a new point $r' = g(r)$ in the deformed image. Using contin-

uous approximations for the image and the deformation function, DIC allows one to study deformations smaller than the image discretization scale, the pixel scale [95, 96].

DIC was first used in the experimental mechanics to measure the deformation field by Sutton [97, 98] and Chu [99]. The method is later utilized for example for measuring crack tip opening angles, displacements and subcritical crack growth [100, 101, 102]. It is also used for estimating the stress intensity factors for 2D and 3D cracks [103, 104]. DIC was applied by Korteoja for measuring the effect of the formation for local strains in paper samples [105].

The image registration algorithm used in this thesis is performed according to the following steps [106, 107]:

- The test image and the deformed image are converted to continuous versions by spline interpolation.
- The algorithm finds a solution to the deformation function between two images.
- The quality of the solution is evaluated by criteria of similarity between the deformed image and a solution g applied to the test image. If the quality of the solution approaches the criteria, it is accepted.

The deformation function is presented as B-splines defined in an evenly spaced lattice, where each piece is determined in a zone of interest, that is, the crate. The B-spline approximation of the deformation function leads to locally minimized elastic energy, and it can represent global affine deformations correctly. The algorithm for the deformation computation is described in [108] and the program is released under GNU Public License. The code derived from the Kybic's thesis has been published as The Google Code project *stdic* in Ref. [109].

An example of the vector field of absolute displacements based on the DIC is shown Fig. 5.3. The displacement is taken from the primary creep regime of a sample whose total time to failure was t_c =1549 s.

One of the approaches to monitor the error of the displacement field was achieved by using different crates: the difference of deformations was computed using two different crates and it was order of 0.003 pixels.

The DIC algorithm accuracy was tested with several approaches. It was compared to a commercially available algorithm, which showed consistent results. The algorithm was tested against a method developed by Korteoja for paper [110]. It was also tested against artificial deformations where the displacement was known exactly. Numerical results from a displacement field were checked with several different methods of computation whenever possible: e.g. comparing the global strain to local strain rates (Publication II). From these tests we concluded that order of 0.1 pixel accuracy was achieved for the absolute displacement measurement. The out-of-plane deformations put a limit to the accuracy, since the paper thickness is the order of 0.1 pixels.

5.2 Acoustic Emission

The strain from an experiment together with acoustic emission (AE) events is presented in the main figure of the Fig. 2.4. In the inset there is a signal from single acoustic emission timeseries, with the events shown.

The AE measurement system consists of a piezoelectric transducer, a rectifying amplifier and continuous data-acquisition. The time-resolution of the measurements is 10 μs and the data-acquisition is free of deadtime. During the experiment bi-polar acoustic amplitudes by a piezocrystal sensor is acquired, as a function of time. The

transducer is attached directly to paper and no coupling agent is used. The data acquisition channel has 12-bit resolution and a sampling rate of 312 000/s. The transmission time from event origin to sensors is in the order of 5 μs. Acoustic channels are first amplified and then saved to a hard disk.

The acoustic time-series was post-processed after the measurement by detection of continuous and coherent events, and the calculation of an event energy E_i is done as the integral of squared amplitudes within the event: $E_i = \int A^2(t')dt'$. The form of the event is due to the measurement device and the physical response of the sample. The envelope forms of are shown in the Fig. 10 of Publication VI, which illustrates a fast raise time and a decaying tail of a typical acoustic emission event.

The event arrival time t_i was taken from the instant when the amplitude raises above the threshold level. The dynamic range of the measurement device was 54 dB. The ensuing discrete set of events is characterized by set of pairs: $\{(t_1, E_1), (t_2, E_2), \ldots\}$. Fig. 2.4 shows a typical acoustic emission from a creep test.

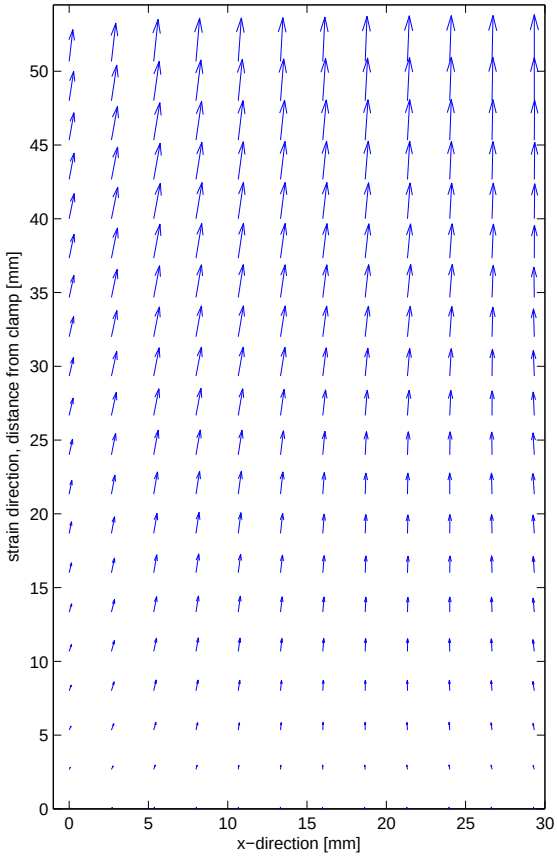

Figure 5.3: Vector field of absolute displacements at $t = 10\,s$ in the creep experiment on paper. Vector lengths are scaled so as to just avoid an overlap and thus show the relative differences of displacement vectors.

6 Results

6.1 Temporal strain rate evolution

In this chapter we investigate the spatial variations in the creep deformation during the primary creep regime. We concentrate on the fluctuation scaling and the interpretation of the strain in the framework of the elastic interface depinning.

The main motivation of the experimental approach in this work is to develop accurate measurement of spatial displacement during creep experiment and study its implications on creep, and the models described. An evenly spaced grid on an image is defined, which consists of a discrete set of points (i, j) with constant spacing Δd. j refers to the strain direction. From the DIC one obtains displacements on each point $\Delta y^{i,j}$ in a time interval dt. A spatial strain rate $\epsilon_t^{i,j}$ in a grid point (i, j) is computed using

$$\epsilon_t^{i,j} = \frac{\Delta y^{i,j'} - \Delta y^{i,j}}{L dt} \tag{6.1}$$

where $L = (j - j')\Delta d$ is the length in which the strain is measured. The distribution $P(\epsilon_t^{i,j})$ ensues, which describes the strain rate evolution during the creep experiment. Examples of the distributions are shown in Fig. 6.1 and the computation is illustrated schematically in the Fig. 2.5.

The samples are found to exhibit a primary creep regime characterized by a power law decay of the average creep strain rate,

$$\langle \epsilon_t^{i,j} \rangle \sim t^{-0.7 \pm 0.1}. \tag{6.2}$$

The spatial variations are found to be characterized by a power law time dependence of the standard deviation of the local strain rates,

$$\Delta \epsilon_t \sim t^{-\gamma}, \tag{6.3}$$

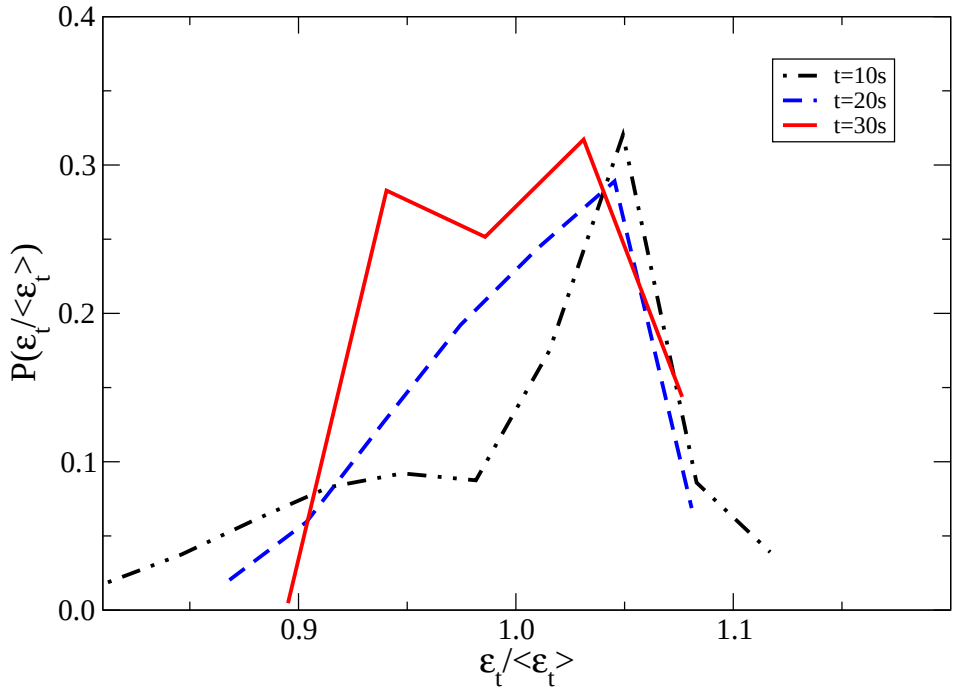

Figure 6.1: The scaled probability distribution functions of strain rates from an experiment, where the time to failure is 1038 s. The width of the distributions increases when time passes. The skewness decreases in this particular sample, but the feature is not observed in all experiments. $L = 14$ mm.

where the fluctuation exponent $\gamma = 0.55 \pm 0.1$ is found. he standard deviation is defined as

$$\Delta\epsilon_t(t) = \sqrt{\frac{1}{N}\sum_{i,j}(\epsilon_t^{i,j}(t) - \langle\epsilon_t^{i,j}(t)\rangle)^2}. \tag{6.4}$$

The magnitude of the fluctuations of the strain rate decay slower with time than the average creep rate, implying that fluctuations become more important in relative terms with time. This experimental finding is presented in Fig. 6.2 and studied in more detail in Publication I. The fluctuation scaling result was independent of the length L used. In the sample scale images during creep, the fluctuation scaling was observed using $L = 14...60\ mm$. The DIC knot spacing of the splines, that is 'crate', being a lower bound and the sample size upper. The DIC analysis on the

magnified images showed the relative strength of the fluctuations increase during creep, when L=0.3 mm. The higher order cumulants were also computed from the distribution $P(\epsilon_t^{i,j})$, but the statistics is insufficient to conclude anything beyond the second order.

When defining and measuring the fluctuations of the strain-field we only study the y component of the strain, defining the relative strain as:

$$\epsilon = \frac{\Delta y}{y}. \tag{6.5}$$

This is a simplification since due to the Poisson's effect transverse strains are observed. This is seen in Fig. 5.3 where we show the vector field of absolute displacements taken from the primary creep regime of a sample whose total time to failure was $t_c = 1549\ s$. The computation of strain rate fluctuations $\Delta\epsilon_t \sim t^{-0.55}$ was also reproduced by using an approximately constant global displacement between images from which the local strain rates $\epsilon_t^{i,j}$ were computed - as opposed to constant image frequency as in Fig. 6.2. This did not change the result of the scaling of strain rate fluctuations. The result was also reproduced by directly studying the relation between the strain rate fluctuations and the strain rate, in order to rule out the effect of a sample-to-sample variation, when averaging the strain rate and the fluctuations over experiments. The result

$$\epsilon_t/\Delta\epsilon_t \sim t^{0.2}$$

was obtained.

The structure of paper exhibits disorder in many scales [111]. In this work we have studied the fluctuations of the strain field during the creep experiment which corresponds to a floc scale and a fibre scale. The floc scale corresponds to the density fluctuations of paper sheet at scales order of 1 cm. The fibre scale emerges from 0.1 mm thick fibres and fibre-fibre bonds. We note that we observed the fluctuation scaling holds from fibre to sheet scale. This suggests that the data needs a model which goes below our observation scale.

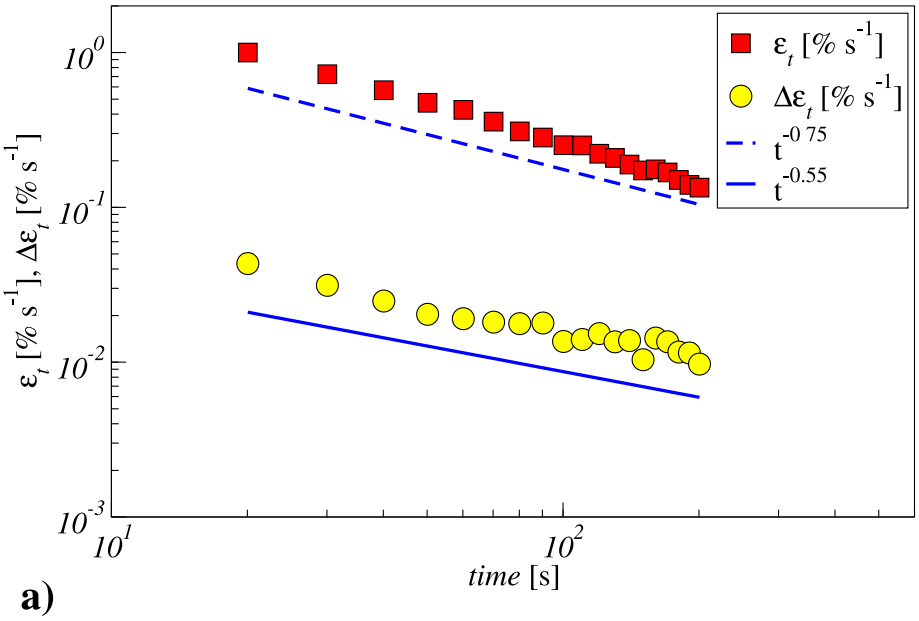

Figure 6.2: Average creep rate and the standard deviation of the local creep rates. Data for a typical set of experiments, that exhibit Andrade's law. The sample average lifetime is 800-1600 seconds. 16 experiments are used to derive the data. The straining volume is $L = 50$ mm. (Publication I)

In Publication I, the creep strain fluctuations are analyzed with the aid of the DDD model. It is shown that the DDD model exhibits a fluctuation scaling law

$$\Delta\epsilon_t^i \sim t^{-0.5}, \tag{6.6}$$

where $\Delta\epsilon_t^i$ is the standard deviation of the local strain rates that are defined by

$$\epsilon_t^i \sim \sum_{\vec{r}_j \in \ box \ i}^{N} b_j v_j, \tag{6.7}$$

where $b_j = \pm 1$ is the magnitude of the Burgers vector and N is the number of boxes.

We give an overview of a model for the creep strain fluctuations by Laurson et al. [112], which is motivated by Cottrell's "strain cages". The model assumes an

intermittent strain activity. Volume elements are divided to "active" and "inactive" during a period Δt. The active boxes are associated with a time dependent strain rate ϵ_t^a, while inactive boxes have strain rate zero. The probability distribution $P(\epsilon_t^{i,j})$ of the local strain rates can be written as

$$P(\epsilon_t^{i,j}) = p(t)\delta(\epsilon_t^{i,j} - \epsilon_t^{a;i,j}) + (1 - p(t))\delta(\epsilon_t^{i,j}), \tag{6.8}$$

where $p(t)$ stands for probability that the box is active. A power law time dependence for both the local strain rate, and probability $p(t)$ is assumed:

$$\epsilon_t^a(t) \sim t^{\alpha' - \Theta},$$

$$p(t) \sim t^{-\alpha'},$$

where $p(t)$ and $\epsilon_t^a(t)$ are chosen so that Andrade's law is fulfilled, that is the average strain rate $\langle \epsilon_t^{i,j} \rangle$ is the number of active boxes Np times strain rate $\epsilon_t^{a;i,j}$, that is

$$\epsilon_t = Np\epsilon_t^{a;i,j} \sim t^{-\Theta}.$$

The standard deviation can now be computed, and it leads to

$$\Delta\epsilon_t^{i,j} \sim t^{\Theta - \alpha/2}.$$

Requiring that the fluctuation scaling exponent $\gamma = \Theta - \alpha/2 \approx 1/2$ agrees with the numerical results, we obtain a self-consistency relation for the number of the active boxes and the strain rate

$$p(t) \sim \epsilon_t^a(t) \sim t^{-1/3}. \tag{6.9}$$

The numerical simulations on the DDD model may be consistent with Eq. (6.9) [112], but experimentally the distributions were intractable with the setup used in this thesis. In both cases, technical difficulties occur. Due to the fact that the strain is a continuous variable, one must perform a thresholding of the strain distribution. The subdivision to boxes, and the definition of the time-scale Δt, in order to choose correct spatial and temporal scales, make the comparison difficult. However, these arguments may provide a way to understand the origins of the fluctuation scaling.

6.2 Interfacial description of the creep deformation

In the interfacial description, the strain is interpreted as the height of the interface $h(x, y; t)$ in depinning models. In the model (Eq. (2.5)) by Zaiser and Moretti the height-height correlation function scales as

$$\sqrt{\langle (h(x + L, y_c) - h(x, y_c))^2 \rangle_x} \sim L^H,$$

where $H = 0.7$ [26]. This approach suggests to test the elastic interface depinning idea further in the spatiotemporal scale.

The elastic interface depinning can be described as a contact process (CP). The contact process exhibits an absorbing state phase transition and belongs to the universality class of directed percolation [113]. The CP is usually defined so that each site of the d-dimensional hypercubic lattice is either vacant or occupied by a particle. Particles are created at vacant sites at a rate $\lambda \sim n/2d$, where n is the number of occupied nearest-neighbours, and are annihilated at unit rate, independent of the surrounding configuration. The order parameter is the particle density ρ and the state, $\rho = 0$, is absorbing. As λ is increased above λ_c, there is a continuous phase transition from the vacuum to an active state. One derives an interfacial model by considering the height of the site $h_i(t)$ to be the total amount of time that the site is occupied (or the number of times it has been active). Dickman and Muñoz conjecture the scaling hypothesis in Eq. (6.10) for the probability density $p(h; t)$ of the height at any lattice site at time t [113]. The mean height is $\langle h(t) \rangle$, and it is expected that

$$p(h; t) = \frac{1}{\langle h(t) \rangle} f(h/\langle h(t) \rangle), \tag{6.10}$$

where f is a scaling function. For the mean height

$$\langle h(t) \rangle \sim t^{1-\theta}, \tag{6.11}$$

which implies that the variance of the height Δh^2 scales as

$$\Delta h^2 \sim t^{2-2\theta}. \tag{6.12}$$

This kind of scaling is expected in models of rough interfaces with the simplest case of spatial and temporal scaling exponents.

Fluctuations in the creep deformation of paper and in DDD are tested against the scaling hypothesis in Eqs. (6.10) and (6.12) in Publication I. In the experiments on paper we measure local relative strains $\epsilon(x, y; t)$ at positions (x, y), where local deformations are computed as displacements between the initial loaded state and at a time t from the initial loaded state. The picture from the initial loaded state is taken 1 second after the load is applied. The scaling hypothesis in the Eq. (6.10) can be applied by interpreting the local deformations $\epsilon(x, y; t) \equiv h(x, y; t)$ as the local heights of an interface and thus the probability density $p(\epsilon; t)$ is expected to scale as the one for the local heights in Eq. (6.10).

Eq. (6.11) corresponds to Andrade's law in the creep experiment and Eq. (6.12) states that, if the scaling hypothesis holds, the variance $\Delta p(\epsilon; t)^2$ of the local deformation distribution scales as:

$$\Delta p(\epsilon; t)^2 \sim t^{\beta'}, \tag{6.13}$$

where $\beta' = 2/3 = 2 - 2\theta$ if the corresponding Andrade's exponent in the Eq. (6.11) is taken as $\theta = 2/3$.

In Fig. 6.3 we depict the scaling functions $f(\epsilon/\langle\epsilon\rangle; t) = \langle\epsilon\rangle p(\epsilon; t)$ during the primary creep in experiments on paper. The deformation data $\epsilon(t)$ is averaged over 16 samples. A similar result for the scaling is obtained from the DDD simulations (Publication I). During the primary creep the variance of fluctuations increase as $\Delta p(\epsilon; t)^2 \sim t^{0.75\pm0.1}$ (experiment) and close to $t^{2/3}$ (simulation). This is shown to support scaling hypothesis in Publication I. One can also extend the experimental data beyond the range in time appropriate for primary creep, with at least rough agreement with the expected behaviour for the secondary creep phase.

Next we analyze the spatial correlation functions of the creep strain field. The

correlation function is defined as a width

$$w(L,t) = \sqrt{\langle(\epsilon(x+L,y_c) - \epsilon(x,y_c))^2\rangle_x}, \tag{6.14}$$

where the roughness of the strain ϵ is averaged over the x coordinate at constant position y_c.

If the elastic interface depinning picture holds, then the scaling behaviour of the width $w(L,t)$ is governed by the scaling relation [114]

$$w(L,t) = t^{1-\Theta} f(\frac{L}{t^{1/z}}), \tag{6.15}$$

where f is scaling function, z is the dynamical exponent and Θ corresponds to Andrade's exponent 2/3.

In the Fig. 6.4 there are squared height-height correlation functions from three different correlation distances L from two typical experiments. We note that for $L = 5mm$ we see approximately Andrade's scaling exponent. The data becomes more inaccurate, when L increases and we are unable to conclude about the form of the scaling function based on the height-height correlations, and further measurements are required for this purpose. However individual and averaged scaling behaviour of the $w(L,t)$ is in agreement with previous results, and provides an independent support for the hypothesis.

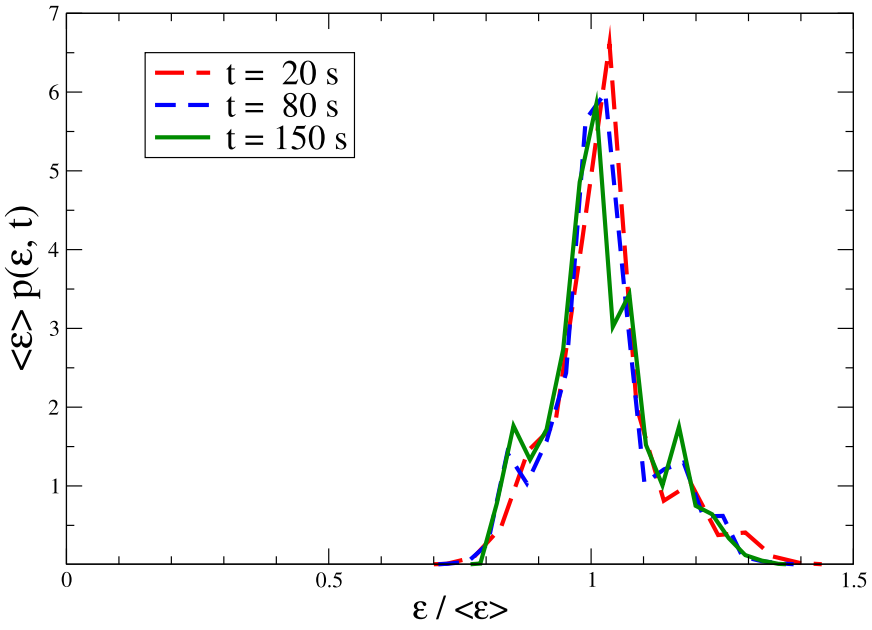

b)

Figure 6.3: Scaling functions of strain fields $f(\epsilon/\langle\epsilon\rangle; t)$ from experiments on paper using $L = 14$ mm. Different lines indicate the time at which f is computed, chosen to be at the beginning, in the middle and at the end of primary creep. The average distribution over 16 different samples is computed by taking all the local displacements at a given time and then computing the scaling function from the distribution $p(\epsilon; t)$. The scaling functions collapse and are consistent with the scaling hypothesis of an absorbing state phase transition (Eq. 6.10). The distributions have a similar asymmetric form and a large-strain tail which is decaying in an exponential fashion. (Publication I)

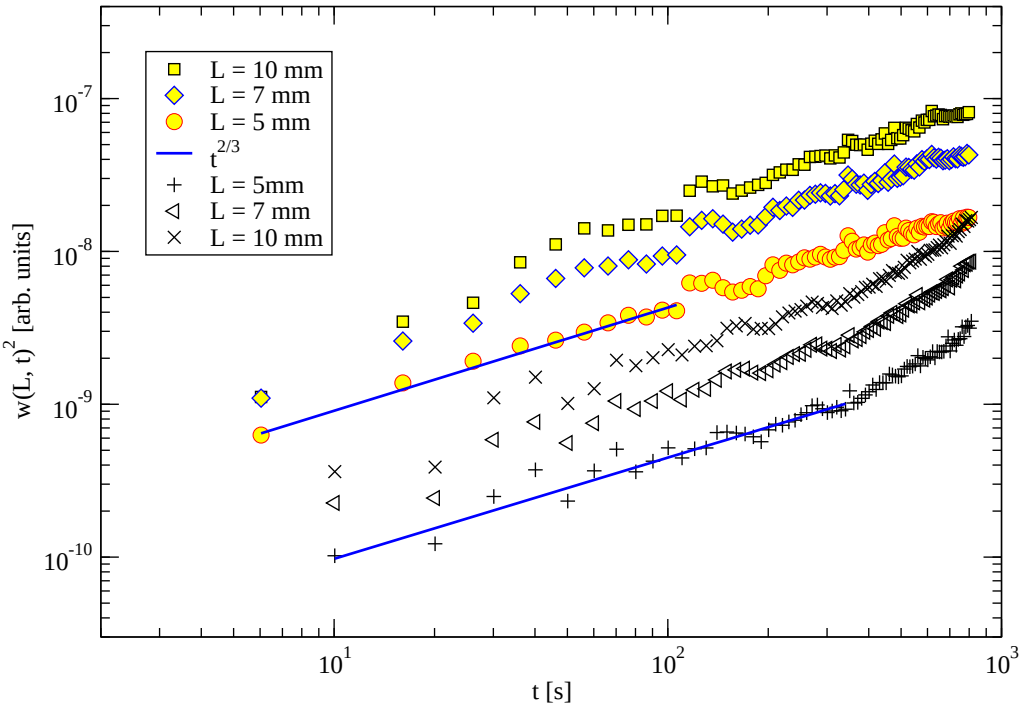

Figure 6.4: Height-heigth correlation functions from experiments. Squared height-height correlation function $w(L,t)^2$ (Eq. 6.15) is consistent with Andrade's law: solid lines are least squares fit to the data. The data shows two typical experiments, where $t_c = 1377s$ and $t_c = 1087s$. The data sets are shifted apart, so the amplitudes are not comparable. When the scale L increases the statistics of the data is insufficient in order to conclude the form of the scaling function $f(L,t)$ in equation 6.15.

6.3 Creep recovery

The creep recovery and the role of spatial variations in the recovered strain (rate) field during creep recovery are studied in detail in the Publication II.

For the creep recovery, the standard deviation $\Delta\epsilon_t$ of the spatial strain rates and the spatial average $\langle\epsilon_t\rangle$ obey the same scaling in time

$$\Delta\epsilon_t \sim \langle\epsilon_t\rangle \sim t^{-1.1}.$$

The result is depicted in the Fig. 6.5.

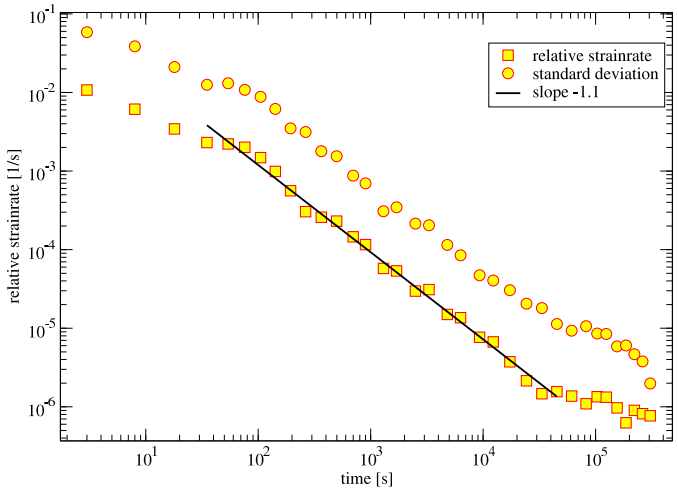

Figure 6.5: Averaged recovery rate ϵ_t and the standard deviation of spatial recovery rates as a function of recovery time. The data is averaged over 32 experiments. The standard deviation shows that the relative width of the recovery rate distribution does not change during the recovery process. (Publication II)

When compared to the primary creep on paper, the relative strength of fluctuations was shown to increase during Andrade's and logarithmic creep. The recovery process does not behave similarly, as the ratio of fluctuations to the mean recovery rate

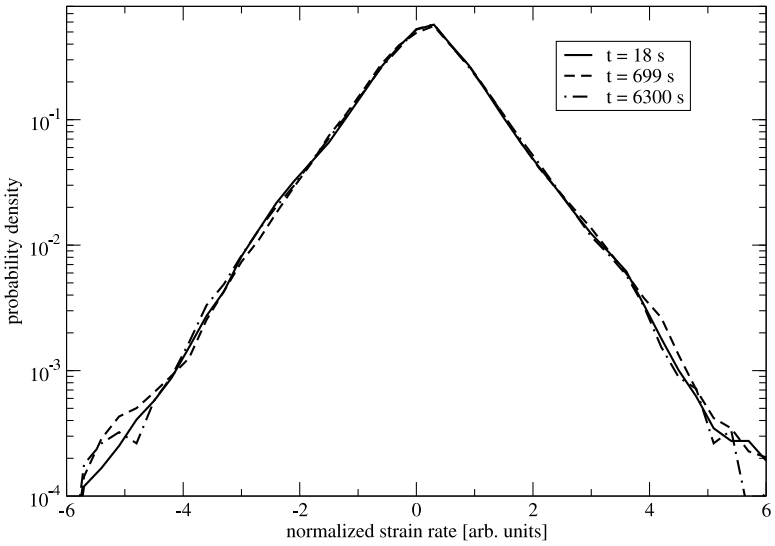

Figure 6.6: Normalized recovery rate distributions averaged over 32 experiments. Comparison of three different recovery times is shown and the distribution is normalized according to $\epsilon'_t = \frac{\epsilon_t - m}{s}$, where m is the average deformation rate and s is the standard deviation of the spatial deformations in the experiment. We see that the average recovery rate and its variations follow the same scaling in time. (Publication II)

is constant. We can test this further by looking at the strain rate probability distribution functions depicted in Fig. (6.6). The distributions are indistinguishable, which is not the case in the creep process.

Thus, despite the fact that we observe a power law recovery, the results suggest strongly that the recovery is not an "inverse Andrade creep" nor an inverse logarithmic creep, as suggested by the jamming transition description of creep in the preceding chapter. The recovery is not driven by critical stress, and the implication is a supporting evidence for the absorbing state transition picture in the primary creep.

Another important consequence of the strain relaxation result is in the context of activation energies: the typical barrier does not increase as a simple exponential decay when the strain rate decreases. While the relative strength of the spatial fluctuations does not increase during the recovery, the mean-field model may be applicable. The fitting model is presented in Publication II, and its main implication is that the largest part of the relaxation of the internal stresses is coming from the elastic stress.

6.4 Damage evolution

In our publications III-VI, we analyze damage accumulation and AE statistics at different loading modes and geometries on a paper sample. In this chapter we will summarize the main results and their implications.

In publication III we present a statistical analysis of acoustic emission (AE) data from tensile experiments on paper sheets, loading mode I, with samples broken under strain control. AE energy release and AE event rates are considered, to test for the presence of "critical points" in fracture, that is the time-to-failure acceleration of the event rate n_t is found to diverge in the creep test:

$$n_t(t_c - t) \sim (t_c - t)^{-\Delta} \tag{6.16}$$

where t_c is time to failure, n_t is the event rate with respect to time and Δ characterizes the acceleration. In Publication III we show that a divergence is observed in strain-controlled tensile experiments, using time as a control parameter and looking at the event rate when approaching time at the maximum event rate. It is shown that the characteristic behaviour of the event energy is different from the event rate, and that the maximum of the event energy and the event rate correspond to a time which is observed after the maximum of the stress in the stress-strain curve. The behaviour of the event rate might be taken to imply criticality, when t_c is chosen to

be the time at the maximum of the event rate. The result of the event rate acceleration is different, when time to maximum stress is considered as "critical point", as it is commonly done. We find the value $\Delta = 1.4 \pm 0.1$ the Eq. (6.16). Earlier experimental studies have shown indications of an event energy divergence when one imposes a constant pressure rate to a heterogenous material [79, 80, 81]. The critical exponent Γ in $E_t \sim \left(\frac{p-p_c}{p_c}\right)^{-\Gamma}$ was found to be $\gamma = 1.4$ in [79], $\Gamma = 1.27$ in [80] and $\Gamma = 1.0$ in [81]. In the case of an imposed constant strain rate there was not found to be any critical divergence of the energy release rate [82, 76]. We point out that, in our experimental results, the most clear sign of the critical behaviour was observed by studying the event rate instead of the energy release rate.

The apparent discrepancy between "criticality" and the exponential increase of the event energy observed by Salminen et al. may be attributed to the brittle nature of the machine direction testing in Ref. [76], in contrast to the cross-machine direction, and ductile stress-strain response, tested in Publication III. Here the "direction" refers to anisotropy in the mechanical properties, due to the manufacturing process of the paper.

We compare the results with the residual random fuse model (RRFN), which is analogous to the one proposed by Duxbury and Li [115]. The model is analogous to the random fuse network [33], but it introduces a residual bonding, leading to apparent plasticity and crack arrest. To get an event rate acceleration in gradual failure by RRFN requires that breaking a fuse creates an "AE event", but accumulating the damage does not. Thus, we find that a gradual failure does not explain an event rate acceleration. Divergent signatures on event rates are not observed in the numerical model.

In Publications IV-VI the dynamics of a "peeling front" or an elastic line is studied under creep (constant load) and constant velocity of the elastic line. The tensile case is reported in Publication IV, and the creep results are published in Publication V

and VI. In the peeling experiments one observes the intermittent dynamics of a crack line as it moves through a sample, largely constrained on a plane. The crack line observes randomness coming from the fibre network structure, a driving force and a self-coupling of the interfacial profile. Under the forced constant velocity of the line, the driving force is coupled to a line movement in a very complicated manner, and experimental results presented in Publication IV do not correspond to any theoretical description.

For a constant driving force f of the crack line in paper peeling, the hypothesis of a depinning transition is tested. A non-equilibrium depinning transition implies a phase diagram for the velocity of the line shown in the Fig. 6.7. The phase diagram depicts the relation between the force and the average velocity of the crack line. The crack line begins to move at a critical value f_c of f such that for $f > f_c$ and $v > 0$ at the zero temperature. Just beyond the critical force, one sees a scaling relation

$$v \sim (f - f_c)^{\beta'}.$$

At larger forces $f \gg f_c$ the effect of the disorder vanishes and one observes a viscous flow.

At finite temperatures, one can show by scaling arguments, or by the functional renormalization group [116] that the velocity of the crack line follows the creep formula

$$v_{creep} \sim \exp\left(-Cf^{-\mu}/T\right). \tag{6.17}$$

The creep formula sets a length scale through thermal activation ($(-Cf^{-\mu}/T) \approx 1$), i.e. it has an Arrhenius form. The equation gives the relation to the driving force f using the creep exponent, μ. The value of the exponent depends on the elastic interactions and the dimensions of the moving object, and we expect

$$\mu = \theta/\nu = \frac{1 - \alpha' + 2\zeta}{\alpha' - \zeta}. \tag{6.18}$$

The exponents θ, ν, and ζ denote the energy fluctuation, correlation length, and equilibrium roughness exponents. For the long range elasticity, one would assume

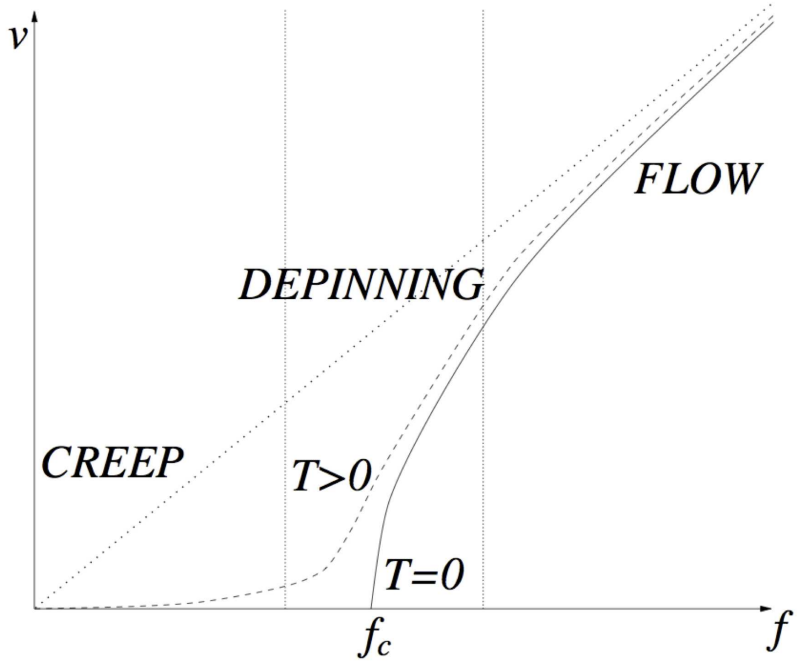

Figure 6.7: Force-velocity relation, exhibiting a creep-depinning phase transition. At $T = 0$ there is discontinuation in the first derivative of the order parameter, i.e. the velocity v, as a a function of the external force. At low forces $f \gg f_c$ and in positive temperatures $T > 0$ the system is in the creep region. From Ref. [93]

$\alpha' = 1$. In Publication V we reported results that show the relationship in line with an Eq. (6.17) as is appropriate for non-local line elasticity with an equilibrium roughness exponent of $\zeta = 1/3$ [93]. In Publication VI it is shown that AE statistics in the peeling experiment is comparable to that of the motion of an elastic line with a long-range elastic force in a random potential.

In Publications III-VI statistical distributions of event energies E_i and inter-event times $\tau = t_{i+1} - t_i$ are analyzed. It appeared that the energy exponent β in the Eq. (4.1) is insensitive to the loading mode in the tensile geometry, the value being in the range $\beta = 1.2...1.4$, which is slightly smaller than models predict [32]. The creep loading mode in the peeling geometry lead to the value $\beta = 1.6 \pm 0.1$. This is comparable to with the Oslo plexiglass experiment, where for the avalanche size,

i.e. the area created by an intermittent event, the value of $\beta = 1.6 \pm 0.1$ was found [86]. The results were compared to simulations where the evolution of an elastic line in a disordered media with the long-range elastic force was studied in Publication VI. The model in the creep regime had an avalanche-like behaviour, but a smaller exponent, $\beta = 1.4 \pm 0.1$, than in the the experimental cases. For a constant strain rate in the paper peeling the value $\beta = 1.8 \pm 0.2$ was found.

These values can be contrasted to the recent analysis by Laurson et al. [117], where it is shown that the avalanche size probability distribution is governed by a local and a global scaling exponent, which are related with a scaling relation $\beta'_{local} = 2\beta_{global} - 1$. The Oslo experiment is shown to follow the result, and the value $\beta'_{local} = 1.5$ is found. The value 1.5 may seem consistent to the result in Publication V for the creep in paper peeling, but it is difficult to argue that the AE energy probability distribution would correspond the local exponent. The numerical models in Publication VI and in Ref. [117] correspond the case of quasi-static external driving of the interface. The quasistatic driving might not be true in the constant strain rate peeling (Publication IV), which may partly explain observed difference in this particular case.

The form of the waiting time distribution $P(\tau)$ implies that correlations are present in the time series, that is the events are not modeled by a Poisson process. In tensile geometries, for creep and constant strain rate loading modes the distribution was closest to power law form (Eq. (4.2)). The analysis of the temporal behaviour in these cases showed that the feature is present only in the time series, which is accumulated over the whole non-stationary experiment. Observations for a quasi-stationary creep in peeling showed that the velocity and the form of the distribution $P(\tau)$ are dependent.

Temporal correlations in the acoustic emission signal are studied further in Publications III-VI. Eq. (6.16) is in essence identical to Omori's law of aftershock rates. In the stationary paper peeling experiment one observes Omori's law with an exponent

close to $\Pi = 1.4$ and it can be contrasted to tectonic seismicity. AE triggered by a line creep in the paper peeling might produce a similar power law relaxation of the foreshock and aftershock rates.

7 Summary and discussion

In this thesis we have tested non-equilibrium statistical physics' ideas against various experimental realizations of damage evolution and fracture. We have utilized the acoustic emission and the digital image correlation methods to extract the data about the phenomena under study.

We have shown that primary creep in tensile geometry can be understood as an absorbing state phase transition, by studying the strain rate which acts as an order parameter, and via the interfacial description of the spatiotemporal evolution of the strain. Moreover, we have discussed the fact that the relative strength of order parameter fluctuations, the standard deviation of the strain rate, increases as a function of time. The results are based on DIC-method. The intermittent nature of a crack front in the paper peeling has been analyzed. Under a constant force, a creep-depinning phase transition has been found by studying the force-velocity relationship of an advancing front.

The elastic interface depinning interpretation of the strain during creep predicts, for example, height-height correlation functions and, due to access to spatial strains, we were able to test the interpretation. In a similar vein, a creep-depinning in paper peeling predicts the form of the correlator and we are able to falsify the creep-depinning framework [118].

By contrasting our experimental results to extensive numerical experiments on the DDD model [50, 52], we have been able to emphasize the universality the elastic interface depinning in a tensile creep. Numerical experiments have also been able to describe the nature of the elasticity of the crack line.

Along with few successes of physics, we have discovered a phenomenology without

understanding. The intermittent spatio-temporal nature of a non-stationary acoustic emission signal from a tensile geometry and constant strain rate peeling serves as an example. There are no testable models that would describe the distributions $P(E)$ and $P(\tau)$ and the correlated dynamics of the crackling noise. However, the experiments on paper may complement experimentally intractable fields, e.g. tectonic seismicity, by providing statistically significant data on experimentally analogous systems.

The experimental setup presented in this thesis was limited to rather slow imaging frequency (1 Hz). Time scales relevant to the acoustic emission event are at the order of millisecond. Increasing the imaging frequency and synchronizing the image data accurately with the acoustic emission might provide a way to observe localized events in the deformation.

A prediction of the failure time in the creep experiment is a problem which has practical importance. Related to the failure prediction, a feature on the creep curve is the Monkman-Grant relation which states that the time at which a minimum creep rate occurs in a sample is proportional to the final failure time [119]. This might be related to the strain fluctuation scaling, since the relative strength of the fluctuations eventually approach the actual strain rate, and it may signal the transition to the tertiary creep. The evidence was not found in the analysis based on the experimental results presented here.

Issue, which is omitted in this thesis, is the effect of the system size. An open question is, if a large scale fracture can be considered physically identical as a smaller scale one [120]. The importance of this question is raised when studying e.g. the dynamics of Arctic sea ice [120]. For example, it is found that the sea ice deformation is heterogenous and intermittent and accommodated by a multiscale and multifractal fracturing process [121, 122, 123]. The analysis of the large scale fracturing process in by using the fluctuation scaling approach or the interfacial framework might

provide a way to understand the size effect of the deformation and the fracture.

References

[1] Z. P. Bazant and F.H. Wittmann, *Creep and Shrinkage in Concrete Structures*, Wiley series in numerical methods in engineering, (1982).

[2] D.W. Coffin, I'Anson, S.J. (ed.), Fundamental Research Conference, Lancashire, UK **39** (2005) 651.

[3] W.N. Findley, *Creep And Relaxation of Nonlinear Viscoelastic Materials*, North-Holland Publishing Company, Amsterdam, (1976).

[4] J.D. Ferry, *Viscoelastic Properties of Polymers*, 3rd Ed., Wiley, (1980).

[5] I.M. Ward and D.W. Hadley, *An Introduction to the Mechanical Properties of Solid Polymers*, Wiley, Chichester, UK, (1993).

[6] K.S. Fancey, J. Mater. Sci. **18** (2005) 4827.

[7] H.E. Stanley, *Introduction to Phase Transitions and Critical Phenomena*, Oxford University Press, (1971).

[8] D. Stauffer and A. Aharony, *Introduction to Percolation Theory*, Taylor and Francis, (1994).

[9] M. Henkel, H. Hinrichsen, and S. Lubeck, *Non-Equilibrium Phase Transitions*, Springer Science, Netherlands, (2008).

[10] B. Mandelbrot, D. Passoja, and A Paullay, Nature **308** (1984) 721.

[11] A-L. Barabasi and H.E. Stanley, *Fractal Concepts in Surface Growth*, Cambridge University Press, Australia, (1995).

[12] E. Bouchaud, Journal of Physics: Condensed Matter **9** (1997) 4319.

[13] J. Kertesz, V.K. Horvath, and F. Weber, Fractals **1** (1993) 67.

[14] L.I. Salminen, M.J. Alava, and K.J. Niskanen, Eur. Phys. J. **B32** (2003) 369.

[15] B. Gutenberg and C. Richter, Bull. Seismol. Soc. Amer. **34** (1944) 185.

[16] F. Omori, J. College Sci. Imper. Univ. Tokyo **37** (1895) 111.

[17] L. da Vinci, *I libri di Meccanica*, Hoepli, Milano, (1540).

[18] J. R. Lund and J.P Byrne, Civil. Eng. and Env. Syst. **18** (2001) 243.

[19] A.A. Griffith, Trans. Roy. Soc. (London) **A221** (1920) 163.

[20] W. Weibull, *A Statistical Theory of the Strength of Materials*, Generalstabens litografiska anstalts förlag, Stockholm, (1939).

[21] D.H. Page, Trend **15** (1969) 7.

[22] M.J. Alava and K.J. Niskanen, Rep. Prog. Phys. **69** (2006) 669.

[23] J. Rosti, L.I. Salminen, E.T. Seppälä, M.J. Alava, and K.J. Niskanen, Eur. Phys. J. **B19** (2001) 259.

[24] E. N. da C. Andrade, Proc. R. Soc. **A84** (1910) 1.

[25] F. Louchet and P. Duval, Int. J. Mat. Res. **100** (2009) 1433.

[26] M. Zaiser and P. Moretti, J. Stat. Mech.: Theo. Exp. **P08004** (2005) 0.

[27] J. Weiss and D. Marsan, Science **89** (2003) 299.

[28] J. Weiss and J-R. Grasso, J. Phys. Chem. B **101** (1997) 6113.

[29] B. Jakobsen et al., Science **312** (2006) 889.

[30] J. Sethna, K. Dahmen, and C. Myers, Nature **410** (2001) 242.

[31] K. Ono, J. Acoustic Emission **12** (1994) 177.

[32] M.J. Alava, P.K.V.V. Nukala, and S. Zapperi, Advances in Physics **55** (2006) 349.

[33] H. Herrmann and S. Roux, *Statistical Models for the Fracture of Disordered Media*, Elsevier Science Publishers, Amsterdam, North Holland, (1990).

[34] J. Rosti, X. Illa, J. Koivisto, and M.J. Alava, J. Phys. D: Appl. Phys. **42** (2009) 214013.

[35] I.M. Ward and D.W. Hadley, *Plastics Engineering*, 3rd edition, Butterworth-Heinemann, Oxford, (1998).

[36] F.R.N. Nabarro and F.De. Villiers, *Physics of Creep and Creep-Resistant Alloys*, CRC, (1995).

[37] P. Duval, Ann. Geophys. **32** (1976) 335.

[38] J.P. Brezinski, Tappi Journal **39** (1956) 116.

[39] C. Crussard and J. Friedel, *Creep and Fracture of Metals at High Temperatures*, HM Stationary Office, London, (1956).

[40] C. Crussard, Proc. R. Soc. Lond. A **371** (1980) 139.

[41] A.H. Cottrell and V. Aytekin, Nature **160** (1947) 328.

[42] N. F. Mott, Proc. R. Soc. Lond. A **220** (1953) 1.

[43] A.H. Cottrell, Phil. Mag. Lett. **B6** (1998) 13.

[44] M.C. Miguel, A. Vespignani, S. Zapperi, J. Weiss, and J-R. Grasso, Nature **410** (2001) 667.

[45] D.M. Dimiduk, C. Woodward, R. LeSar, and M.D. Uchic, Science **312** (2006) 1188.

[46] F. Csikor et al., Science **318** (2007) 251.

[47] A.J. Liu and S. R. Nagel, Nature **396** (1998) 21.

[48] J. Goyon et al., Nature **454** (2008) 84.

[49] A.S. Keys et al., Nature Phys. **3** (2007) 260.

[50] M.C. Miguel, A. Vespignani, M. Zaiser, S. Zapperi, Phys. Rev. Lett. **89** (2002) 165501.

[51] L. Laurson, M.C. Miguel, and M.J. Alava, Phys. Rev. Lett. **105** (2010) 015501.

[52] L. Laurson, M.C. Miguel, M.J. Alava, Eur. Phys. J. **B64** (2008) 443.

[53] G.S. Daehn, Acta mater. **49** (2001) 2017.

[54] P. Bak, C. Tang, and K. Wiesenfeld, Phys. Rev. A **38** (1988) 364.

[55] M. Zaiser, F. Madani, V. Koutsos, and E.C. Aifantis, Phys. Rev. Lett. **93** (2004) 195507.

[56] A.H. Cottrell, J. of Mech. and Phys. of Sol. **1** (1952) 53.

[57] C.L. Smith, Proc. Phys. Soc. **61** (1948) 201.

[58] N.F. Mott and F.N.R Nabarro, *Report on a Conference on the Strength of Solids*, Physical Society of London, (1948).

[59] M. Pecht, M.W. Johnson, and R.E. Rowlands, Tappi Journal **67** (1984) 106.

[60] J. Van den Akker, Tappi Journal **33** (1950) 398.

[61] H. W. Haslach, Jr., Mech. Time-Dep. Mat. **4** (2000) 169.

[62] W.N. Findley, Polymer Eng. and Sci. **27** (2007) 582.

[63] Y. Nakumara, C.L. Veach, and B.O. McCauley, *Acoustic Emission*, Am. Soc. for Test. and Mat. ST-505, (1972).

[64] D.O. Thompson and D.E. Chimenti, *A Review of Progress in Quantitative Nondestructive Evaluation*, A Division of Plenum Publ. Corp., (1997).

[65] R.K. Miller and P.McIntire, *Acoustic Emission Testing*, Am. Soc. for Nondest. Test., (1997).

[66] F. Finck, M. Yamanouchi, H-W. Reinhardt, and C.U. Grosse, Int. J. Fract. **124** (2003) 139.

[67] H. Corte and O. Kallmes, *Formation and Structure of Paper*, Publ. Ltd. London, (1962).

[68] T. Yamauchi, S. Okumara, and N. Noguchi, J. Pulp Paper Sci. **16** (1990) 14.

[69] T. Yamauchi and K. Murakami, Tappi J. **76** (1993) 101.

[70] T. Fuketa, S. Okumura, M. Noguchi, and T. Yamauchi, J. Acoustic Emission **11** (1993) 21.

[71] P. Gradin, S. Nyström, P. Fling, S. Forsberg, and F. Stollmaier, J. Pulp Paper Sci. **23** (1997) 113.

[72] J. Rosti, *Acoustic Emission During Tensile Straining of Paper*, Master's Thesis, Helsinki University of Technology, Department of Engineering Physics and Mathematics, (1999).

[73] L.I. Salminen, *Aspects of Fracture Processes in Paper*, Ph.D. Thesis, Helsinki University of Technology, Otamedia, Espoo, (2003).

[74] K. Mogi, Bull. Earthq. Res. Inst. **40** (1962) 125.

[75] A. Petri, G. Paparo, A. Vespignani, A. Alippi, and M. Costantini, Phys. Rev. Lett. **73** (1994) 3423.

[76] L.I. Salminen, A.I. Tolvanen, and M.J. Alava, Phys. Rev. Lett. **89** (2002) 185503.

[77] C. Maes, A. Van Moffaert, H. Frederix, and H. Strauven, Phys. Rev. B. **57** (1998) 4987.

[78] S. Deschanel, L. Vanel, N. Godin, G. Vigier, and S. Ciliberto, Int. J. Fract. **140** (2006) 87.

[79] A. Johansen and D. Sornette, Ann. Geophys. **32** (1976) 335.

[80] A. Garcimartin, A. Guarino, and S. Ciliberto, Phys. Rev. Lett. **79** (1997) 3203.

[81] H. Nechad, A. Helmsletter, R Guerjouma, and D. Sornette, Phys. Rev. Lett. **94** (2005) 045501.

[82] A. Guarino, A. Garcimartin, and S. Ciliberto, Eur. Phys. J. **B6** (1998) 13.

[83] A. Guarino, S. Ciliberto, A. Garcimartin, M. Zei, and R. Scorretti, Eur. Phys. J. **B26** (2002) 141.

[84] A. Petri, Phil. Mag. **77** (1998) 491.

[85] S. Deschanel, L. Vanel, N. Godin, G. Vigier, and S. Ciliberto, J. Stat. Mech. **2009** (2009) P01018.

[86] K. J. Måløy, S. Santucci, J. Schmittbuhl and R. Toussaint, Phys. Rev. Lett. **96** (2006) 045501.

[87] P. Le Doussal, K. J. Wiese, S. Moulinet, and E. Rolley, Europhys. Lett. **87** (2009) 56001.

[88] A. B. Kolton, A. Rosso, and T.Giamarchi, Phys. Rev. Lett. **94** (2005) 047002.

[89] S. Lemerle, J. Ferré, C. Chappert, V. Mathet, T. Giamarchi, and P. Le Doussal, Phys. Rev. Lett. **80** (1998) 849.

[90] G. Blatter, M.V. Feigelman, V.B. Geshkenbein, A.I. Larkin, and V.M. Vinokur, Rev. Mod. Phys. **66** (1994) 1125.

[91] T. Nattermann, Y. Shapir, and I. Vilfan, Phys. Rev. B **42** (1990) 8577.

[92] A. B. Kolton, A. Rosso, and T.Giamarchi, Markov Processes Relat. Fields **13** (2007) 777.

[93] P. Chauve, T. Giamarchi, and P. Le Doussal, Phys. Rev. B **62** (2000) 6241.

[94] P. Le Doussal, K. Wiese, J. Kay, and P. Chauve, Phys. Rev. B **66** (2002) 174201.

[95] J.C. Duprè, EPJ Web of Conferences **6** (2010) 31006.

[96] M. Bornent et al., Exp. Mech. **49** (2009) 353.

[97] M.A. Sutton, W.J. Wolters, W.H. Peters, W.F. Ranson, and S.R. McNeill, Image Vis. Comput. **1** (1983) 133.

[98] M.A. Sutton, J.L. Turner, H.A. Bruck, and T.A. Chae, Exp. Mech. **31** (1991) 168.

[99] T.C. Chu, W.F. Ranson, M.A. Sutton, and W.H. Peters, Exp. Mech. **3** (1985) 324.

[100] D.S. Dawicke, M.S. Sutton, Exp. Mech. **34** (1994) 357.

[101] P. Forquin, L. Rota, Y. Charles, and F. Hild, Int. J. Fract. **125** (2004) 171.

[102] J. Koivisto, *Sub-critical crack propagation*, Master's Thesis, Helsinki University of Technology, Department of Engineering Physics and Mathematics, (2007).

[103] S. Roux and F. Hild, Int. J. Fract. **140** (2006) 141.

[104] S. Roux, J. Rethore, and F. Hild, J. Phys. D. **42** (2009) 214004.

[105] M.J. Korteoja, K.J. Niskanen, K. Kaski, and M.T. Kortschot, *Progressive Damage in Paper*, *Research report: B6, ISSN 1455-0474, ISBN 951-22-3616-8*, Laboratory of Computational Engineering, Helsinki University of Technology. Espoo, (1997).

[106] J. Kybic and M. Unser, IEEE Trans. Image Process. **12** (2003) 1427.

[107] J. Kybic, *Elastic Image Registration using Parametric Deformation Models*, PhD Thesis, Ecole Polytech. Fed. Lausanne, (2001).

[108] J. Kybic, P. Thevenaz, A. Nirkko, and M. Unser, IEEE Trans. on Med. Imag. **19** (2000) 80.

[109] Google Code Project, *DIC software*, http://code.google.com/p/stdic/, (18.8.2010).

[110] M.J. Korteoja, *Damage and Fracture in Fibrous Compounds: the Effect of Structural Disorder*, Ph.D. Thesis, Helsinki University of Technology, Espoo, (1997).

[111] K.J. Niskanen, *Paper Physics*, Fapet Oy, Helsinki, Finland, (1998).

[112] L. Laurson et al., (in preparation) .

[113] R. Dickman and M.A. Muńoz, Phys. Rev. E **62** (2000) 7632.

[114] J. M. López, Phys. Rev. Lett. **83** (1999) 4594.

[115] Y. Li and P. M. Duxbury, Phys. Rev. B. **38** (1988) 9257.

[116] P. Chauve, T. Giamarchi, and P. Le Doussal, Europhys. Lett. **44** (1998) 110.

[117] L. Laurson, S. Santucci, and S. Zapperi, Phys. Rev. E **81** (2010) 046116.

[118] J. Koivisto et al., (in preparation) .

[119] F.C. Monkman and N.J. Grant, Proc. ASTM **56** (1956) 593.

[120] E.M. Schulson and P. Duval, *Creep and Fracture of Ice*, Cambridge, eBook: www.cambridge.org/9780521806206, (2009).

[121] P. Rampal, J. Weiss, D. Marsan, R. Lindsay, and H. Stern, J. Geo. Res. **112** (2008) C03002.

[122] P. Rampal, J. Weiss, D. Marsan, and M. Bourgoin, J. Geo. Res. **114** (2009) C10014.

[123] A. Cheml, V.N. Smirnov, and I.B. Sheikin, Ocean Sci. Discuss. **6** (2009) 1595.

ISBN 978-952-60-3458-4
ISBN 978-952-60-3459-1 (PDF)
ISSN 1795-2239
ISSN 1795-4584 (PDF)